



This is a repository copy of *Comparison of TCD and SED methods in fatigue lifetime assessment*.

White Rose Research Online URL for this paper:
<http://eprints.whiterose.ac.uk/142394/>

Version: Accepted Version

Article:

Hu, Z., Berto, F., Hong, Y. et al. (1 more author) (2019) Comparison of TCD and SED methods in fatigue lifetime assessment. *International Journal of Fatigue*, 123. pp. 105-134. ISSN 0142-1123

<https://doi.org/10.1016/j.ijfatigue.2019.02.009>

Article available under the terms of the CC-BY-NC-ND licence
(<https://creativecommons.org/licenses/by-nc-nd/4.0/>).

Reuse

This article is distributed under the terms of the Creative Commons Attribution-NonCommercial-NoDerivs (CC BY-NC-ND) licence. This licence only allows you to download this work and share it with others as long as you credit the authors, but you can't change the article in any way or use it commercially. More information and the full terms of the licence here: <https://creativecommons.org/licenses/>

Takedown

If you consider content in White Rose Research Online to be in breach of UK law, please notify us by emailing eprints@whiterose.ac.uk including the URL of the record and the reason for the withdrawal request.



eprints@whiterose.ac.uk
<https://eprints.whiterose.ac.uk/>

Comparison of TCD and SED methods in fatigue lifetime assessment

Zheng Hu^{a,d}, Filippo Berto^b, Youshi Hong^c, Luca Susmel^{d,*}

^aScience and Technology on Vehicle Transmission Laboratory, China North Vehicle Research Institute, Beijing 100072, China

^bNorwegian University of Science and Technology, NO-7491 Trondheim, Norway

^cInstitute of Mechanics, Chinese Academy of Sciences, Beijing 100190, China

^dDepartment of Civil and Structural Engineering, The University of Sheffield, Mappin Street, Sheffield S1 3JD, UK

Abstract

This paper assesses the accuracy and reliability of the Theory of Critical Distances (TCD) and the Strain Energy Density (SED) approach in estimating the lifetime of plain and notched specimens subjected to cyclic loading. To validate the two approaches for plain and notched components under uniaxial and multiaxial fatigue loading, a large bulk of experimental data taken from the literature were re-analyzed, with the state variables, i.e. the stress distributions and the strain energy density, being calculated via Finite Element (FE) approach. The results obtained demonstrate that both the TCD and the SED approach can provide highly accurate fatigue life estimation. In addition, the two adopted approaches require few computational efforts and experimental data to be implemented and used for fatigue design in situations of practical interest.

Keywords: Theory of Critical Distances, Strain Energy Density, Modified Wöhler Curve, Uniaxial fatigue, Multiaxial fatigue.

Nomenclature

k, k_{τ}	negative inverse slope of the Wöhler curve	E	elastic modulus
K_{th}	threshold value of the stress intensity factor	$\Delta\sigma_{p,el}$	elastic peak stress ranges at the notch tip under tension loadings
K_t	stress concentration factor	$\Delta\sigma_{nom}$	nominal stress ranges tied to tension loadings,
K_{IC}	plane strain material toughness	σ_0	plain fatigue limit
$K_{t,net,axial}$, $K_{t,net,torsional}$	theoretical stress concentration factors under tension and torsion loadings	σ_{eff}	effective stress calculated according to the TCD
ΔK_{1A} , ΔK_{3A}	reference values at high cycle fatigue of the notch stress intensity factor range under Mode I and III loading	σ_1	maximum principal stress

K_1, K_2, K_3	the values of mode I, mode II and mode III NSIF	σ_u	ultimate tensile stress
L	material characteristic length	σ_A	amplitude of the nominal gross stress at N_A cycles
L_M	material characteristic length determined in the medium-cycle fatigue regime	$\sigma_{g,a}$	amplitude of the nominal gross stress
N_0	number of cycles to failure defining the position of the knee point	$\sigma_{1,a}$	amplitude of the maximum principal stress
N_f	number of cycles to failure	$\sigma_{n,m}$	mean stress perpendicular to the critical plane
N_A	reference number of cycles to failure in the high-cycle fatigue regime	$\sigma_{n,a}$	amplitude of the stress perpendicular to the critical plane
$N_{f,e}$	estimated number of cycles to failure	$\sigma_{A,p}$	fatigue strength of the smooth sample at N_A cycles
I_1, I_2	the first and second invariants of the stress tensor	σ_{ij}	stress state components
R_0	radius of the control volume	σ_0	fully reversed uniaxial fatigue limit
R	load ratio	$\sigma_{A,n}$	nominal stress of notch sample at N_A cycles
R_1, R_3	the radius of the control volume under Mode I and Mode III loading	$\Delta\sigma_A$	nominal stress range of the unnotched material
r, θ	polar coordinates	$\Delta\tau_{p,el}$	elastic peak stress ranges at the notch tip under torsion loadings
m	mean stress sensitivity index	$\Delta\tau_{nom}$	nominal stress ranges tied to torsion loadings,
$\overline{\Delta W}_0^{plain}$	strain density energy from the plain sample	$\lambda_1, \lambda_2, \lambda_3$	Williams' eigenvalues
$\overline{\Delta W}^{notch}$	strain energy density value averaged over the control volume from the notch sample	e_1, e_2, e_3	shape functions for sharp V-notches
W_c	critical energy value	2α	opening angle of notch
$W_{element,i}$	energy contributions for all the finite element	ν	Poisson's ratio
$\overline{\Delta W}$	averaged value of the SED over a control volume	c_w	weighting parameter
τ_0	fully reversed torsional fatigue limit	V	control volume
τ_a	maximum shear stress amplitude	T_σ, T_W	stress-based and strain energy-based scatter index
$\tau_{A,Ref}$	amplitude of the reference shear stress at N_A cycles to failure	a, b, α, β	constants used in the MWCM approach
ρ_{eff}	effective value of the critical	δ_{ij}	Kronecker delta

ρ_{lim}	plane stress ratio limit value of ρ_{eff}	TCD	Theory of Critical Distances
E_N	error of fatigue life calculation	SED,	Strain Energy Density,
ε_{ij}^e	elastic strain state components	MWCM	Modified Wöhler Curve Method

1 Introduction

The fatigue problem of mechanical components has been studied intensively to safely assess structures subjected to different and complex loading conditions. Accurate fatigue damage prediction of structural components is still a big challenge due to a number of variables, including geometrical discontinuities, non-zero superimposed static stresses and the degree of multiaxiality of the stress fields that can change locally near the stress risers. There are numerous methods to predict fatigue life of structural components under different stress conditions [1-4]. However, a universal criterion for plain and notched specimens under uniaxial and multiaxial loading conditions has not yet been agreed by the international scientific community.

In the present study, the accuracy in performing fatigue assessment of the TCD [5-10] and the SED approach [11-18] has been checked systematically against a large number of experimental results taken from the literature.

The elastic maximum stress at the notch tip can be successfully used only to assess the fatigue strength of blunt notches. When notches become sharp, the assessment based on the maximum value of the stress evaluated at the notch tip are invariably too conservative. Many different strategies have been employed to evaluate the detrimental effect on the material fatigue strength of blunt and sharp notches. Based on the critical distance concept, Neuber [19] and Peterson [20] were able to estimate the high-cycle fatigue strength of mechanical components experiencing stress concentration. Tanaka [21], Lazzarin et al. [22] and Taylor [23] proposed a closed form relationship between the critical distance and El Haddad's length parameter [24]. Both the TCD and SED approach assume that engineering materials obey a linear-elastic constitutive law and the linear-elastic stress fields of interest can be easily evaluated by using simple linear-elastic FE solutions that are able to capture with high accuracy the stress field in the vicinity of the stress concentrator being investigated. By employing the TCD, the fatigue behavior of notched components can be predicted from such stress fields by using two material parameters: characteristic length L and the plain material fatigue limit. The idea of a microstructural support is due to Neuber [19]. Afterwards, Susmel and Taylor reviewed most of the findings in the use of the TCD to assess the fatigue strength of notched mechanical

components [25-27]. They were able to validate the accuracy of the TCD when applied to the fatigue assessment of specimens weakened by notches under cyclic variable loading conditions. Recently, in conjunction with the TCD, the Modified Wöhler Curve Method (MWCM) was successfully employed in predicting the finite lifetime of notched components subjected to complex loadings [7, 8, 28-30]. The proposed fatigue life estimation technique is based on the assumption that the linear elastic stress state can be used to estimate the fatigue damage, at least when the fatigue phenomenon is governed by the initiation phase and the propagation phase is limited. In addition, the MWCM directly considers the degree of multiaxiality of the stress field in a process zone placed in the proximity of the notch tip. At the same time, the degree of multiaxiality of the stress field damaging the fatigue process zone is directly accounted for the MWCM, which is a critical plane approach sensitive to the presence of both non-zero mean stresses and non-proportional loadings.

Some methodologies making use of the energy density have also been used to assess the fracture and fatigue behavior of materials exhibiting both ductile and brittle behavior. Different SED-based approaches were proposed and applied to static and fatigue loading conditions [31-38]. Dealing with the strain energy density concept, Sih proposed a criterion based on the strain energy density factor S , which is a point method criterion and determine the direction of crack propagation by imposing a minimum condition on S [32, 39-41]. A more general formulation, based on a fatigue master curve evaluated from the sum of the positive elastic and plastic strain energy densities of representative cyclic hysteresis loops, was suggested by Ellyin et al. In some uniaxial and multiaxial cyclic fatigue results, the SED-based approaches can accurately assess the fatigue behavior of components [42-45]. Lazzarin et al. firstly introduced the concept of mean strain energy density, which is evaluated over a control volume surrounding the notch tip [11, 46-48]. The method derived from the elementary structural volume concept previously proposed by Neuber [19]. The control radius of the volume is a material property: in the case of static loading, it depends on the ultimate tensile strength, the fracture toughness and Poisson's ratio; in the case of high cycle fatigue loading, it also depends on the unnotched specimen's fatigue limit and the threshold stress intensity factor range. The main advantage of the averaged SED over the local stress-based criteria is the mesh independency and insensitive to the mesh refinement. For this reason, a method to rapidly estimate the averaged SED at the tip of cracks under in-plane mixed mode loading has been recently proposed. It is based on the peak stresses evaluated from finite element (FE) analyses, according to the peak stress method [49-51]. The averaged SED has been found to be one of the most powerful tools to assess the static and

fatigue behaviour of notched and unnotched components in structural engineering [40, 41, 52-58].

In this paper, the aim is to investigate the accuracy of TCD and SED methods in estimating fatigue life of plain and notched specimens under uniaxial and multiaxial loading. Firstly, the framework of TCD and SED methods for notched components under uniaxial fatigue loading are described. A large number of experimental data relevant to blunt and sharp notched specimens have been employed herein for the validation purpose. In the second part of the work, the analytical frames of the same criteria for multiaxial fatigue loading are introduced. Validations are given by comparing the predictions with a large number of experimental data from different materials and involving samples under different loading conditions. Finally, conclusions are drawn.

2 Fatigue assessment of notched components under uniaxial fatigue loading

2.1 Fatigue lifetime estimation of notched components using TCD

Peterson [20] proposed the point method (PM) which considers as a critical parameter the effective stress measured at a given distance from the tip from the stress raiser. On parallel tracks, the line method (LM) was formalized by Neuber [19]. The LM method is based on the idea that the effective stress is averaged over a line. These methods have been successfully formalized by taking into account the LEFM concepts [21-23].

The material characteristic length L can be evaluated as follows as:

$$L = \frac{1}{\pi} \left(\frac{K_{th}}{\sigma_0} \right)^2 \quad (1)$$

where K_{th} is the threshold value of the stress intensity factor and σ_0 is the plain fatigue limit of material (both determined at the same load ratio, R , applied to the specimens). As briefly mentioned above, the TCD can be formalized in different ways, by considering different integration domains (point, line, area or volume method) for the effective stress σ_{eff} evaluation. Under the mode I loading conditions, the PM postulates that the effective stress is equal to the principal stress measured at a distance from the notch tip equal to $L/2$. The critical condition is reached when $\sigma_{eff} = \sigma_0$ as explicitly reported below:

$$\sigma_{eff} = \sigma_1 \left(\theta = 0, r = \frac{L}{2} \right) = \sigma_0 \quad (2)$$

In Eq. (2) σ_1 is the maximum principal stress, θ and r are the polar coordinates. The value of σ_1 should be evaluated along a line drawn starting from the hotspot (the point experiencing the maximum peak

stress) in a direction normal to the maximum principal stress. Usually, this direction is normal to the surface of the notched components. Under mode I loading conditions, the notch bisector represents the line of stress evaluation.

Instead of determining σ_{eff} at a given distance from the notch tip, the LM can be evaluated by averaging the value of σ_1 along the notch bisector over a distance equal to $2L$ at the fatigue limit condition of the notched component:

$$\sigma_{\text{eff}} = \frac{1}{2L} \int_0^{2L} \sigma_1(\theta=0, r) dr = \sigma_0 \quad (3)$$

For the area and volume method, the range of the effective stress can be calculated by averaging the principal stress over a semicircular area of radius equals to L (area method) or in a hemisphere centered at the notch tip with the radius equal to $1.54L$ (volume method) [59].

As an extension to the finite fatigue lifetime, Susmel and Taylor proposed to apply the TCD in medium-cycle fatigue regime by considering the critical distance, L , as material property but also as a function of the number of cycles to failure. The following expression has been proposed in Ref [25]:

$$L_M(N_f) = A \cdot N_f^B \quad (4)$$

In Eq. (4) A and B are material constants to be determined by running appropriate experiments, which require some simple static tests to determine the ultimate tensile stress σ_u and plane strain material toughness K_{IC} and some standard fatigue tests aimed to determine the plain fatigue limit σ_0 and the threshold value of the stress intensity factor K_{th} . Unfortunately, the stress based approach is not adequate at describing the behavior of engineering materials in the low-cycle fatigue regime, resulting in an approximate calculation of the reference number of cycles to failure in the low-cycle fatigue regime. Besides, it is very difficult to coherently define the reference number of cycles to failure in the high-cycle fatigue regime corresponding to the knee point due to the fact that, for a given material, the position of the knee point can change by changing the geometry of the tested samples. So it is not adequate to determine constants A and B by using the above strategy.

In order to overcome the just mentioned problem, an alternative proposed by Susmel and Taylor [25] was adopted. This proposal is based on two calibration σ - N fatigue curves: one obtained by testing plain specimens and the second one obtained by testing notched specimens. In particular, by using the PM, the values of $\sigma_{1,a}$ can be determined at any given number of cycles N_f by the Wöhler equation (see Fig. 1):

$$\sigma_A^k N_A = \sigma_{1,a}^k N_f \quad (5)$$

In Eq. (5) N_A is reference number of cycles to failure in the high-cycle fatigue regime and σ_A is the amplitude of the nominal gross stress at N_A cycles. The linear elastic stress field distribution in the proximity of the notch tip can be determined by FE method. The mapped mesh in the vicinity of the stress raiser's apex is gradually refined until convergence occurred. Then, the linear elastic stress field distribution $\sigma_1(r)$ can be fitted accurately with an exponential decay function (coefficient of determination: $R^2 > 0.99$) through a post processing of the simulated data. For the calculated values, it is easy to determine the distance $L_M(N_f)/2$ from the fitting function.

$$\sigma_{1,a} = \sigma_1 [L(N_f)/2] \quad (6)$$

An identical procedure can be used to evaluate the distance $2L_M(N_f)$ with the LM:

$$\sigma_{1,a} = \frac{1}{2L} \int_0^{2L} \sigma_1(\theta=0,r) dr = \frac{1}{2L_M(N_f)} \int_0^{2L_M(N_f)} \sigma_1(\theta=0,r) dr \quad (7)$$

By calculating the critical distance value for all the numbers of cycles, constants A and B in Eq. (4) can be determined by employing a fitting procedure.

In order to better clarify the recursive procedure which can be used to assess the number of cycles to failure $N_{f,e}$ by using the TCD, consider a notched specimen subjected to a given value of the nominal stress $\sigma_{g,a}$. The distribution of the linear elastic stress field can be determined by using a FE model. Then by simply substituting the equation $L_M = A \cdot N_{e,f}^B$ into Eq. (6), it is possible to write:

$$\sigma_1(r) = \sigma_1 [L(N_{e,f})/2] = \sigma_1 [A \cdot N_{e,f}^B / 2] = \sigma_{1,a} \quad (8)$$

Subsequently, by substituting the value of $\sigma_1 [L(N_{e,f})/2]$ into the Eq. (5), the equation just containing the number of cycles to failure $N_{f,e}$ can be obtained:

$$N_{e,f} = N_A \cdot \left(\frac{\sigma_A}{\sigma_{1,a}} \right)^k = N_A \left(\frac{\sigma_A}{\sigma_1 [L(N_{e,f})/2]} \right)^k = N_A \left(\frac{\sigma_A}{\sigma_1 [A \cdot N_{e,f}^B / 2]} \right)^k \quad (9)$$

Through Newton's method, the value of $N_{f,e}$ can be determined directly from Eq. (9) which provides a general solution. If Eq. (9) does not have a real root, an approximate value obtained by minimizing the error can be obtained. The same procedure can be used for applying the LM with the only difference that in Eq. (9) the integral form is still present as shown below:

$$N_{e,f} - N_A \cdot \left(\frac{\sigma_A}{\frac{1}{2A \cdot N_{e,f}^B} \int_0^{2A N_{e,f}^B} [\sigma_1(r)] dr} \right)^k = 0 \quad (10)$$

The relationship between L_M and N_f can be obtained by testing plain and V-notched specimens. The main advantage of this approach is its accuracy in determining L and the possibility to be easily applied to engineering applications. For different geometrical features, under the hypothesis of linear elasticity and at high-cycle regime, the use of notches as sharp as possible is always recommended to generate the fatigue curve needed to determine the main constants A and B .

The two calibration σ - N fatigue curves can be used to assess the fatigue life of other notched specimens made of the same material and tested at the same load ratio. The procedure mainly consists in defining the L_M versus N_f relationship based on the use of two calibration curves and consequently finding the linear elastic stress field distribution along the distance under at a given nominal stress $\sigma_{g,a}$ by FE method. Finally, the estimation is based on PM or LM by substituting the linear elastic stress field distribution into Eq. (9) or Eq. (10). Such the method is also summarized by the flow-chart sketched in Fig. 2.

2.2 Estimate fatigue lifetime of notched components using SED

The local SED approach has been extensively used in the last years to deal with high cycle fatigue of notched components and welded joints. The local SED states that failure occurs when the mean value of the strain energy density averaged over a control volume surrounding the notch tip is equal to a critical energy value W_c . Under plane strain or plane stress conditions, the control volume becomes a circle, a circular sector or a crescent shape as depicted in Fig. 3, where the radius of the control volume R_0 does not depend on the notch geometry. Under the hypothesis of plane strain, all the stress and strain components in the highly stressed region are related to mode I and II notch stress intensity factors (NSIFs). The expressions for the NSIFs can be defined according to the following expressions:

$$K_1 = \sqrt{2\pi} \lim_{r \rightarrow 0^+} r^{1-\lambda_1} \sigma_{\theta\theta}(r, \theta = 0) \quad (11)$$

$$K_2 = \sqrt{2\pi} \lim_{r \rightarrow 0^+} r^{1-\lambda_2} \tau_{r\theta}(r, \theta = 0) \quad (12)$$

Thus, the strain energy in a well defined area surrounding the notch tip as shown in Fig. 3 can be evaluated as follows:

$$\Delta\bar{W} = \frac{c_w}{E} \left[e_1 \cdot \frac{\Delta K_1^2}{R_0^{2(1-\lambda_1)}} + e_2 \cdot \frac{\Delta K_2^2}{R_0^{2(1-\lambda_2)}} \right] \quad (13)$$

In Eq. (13) λ_1 and λ_2 are Williams' eigenvalues, ΔK_1 and ΔK_2 represent the values of mode I and mode II NSIF ranges, and R_0 represents the radius of the control volume. e_1 and e_2 are shape functions which depend on the notch angle 2α and the Poisson's ratio ν . In order to consider the influence of the nominal load ratio R , the weighting parameter c_w has to be adopted in agreement with the following expression [54, 60]:

$$c_w(R) = \begin{cases} \frac{1+R^2}{(1-R)^2} & \text{for } -\infty \leq R < 0 \\ 1 & \text{for } R = 0 \\ \frac{1-R^2}{(1-R)^2} & \text{for } 0 \leq R < 1 \end{cases} \quad (14)$$

Under uniaxial loading (i.e., mode I loading) the mode II contribution vanishes, Eq. (13) can be simplified as follow:

$$\Delta\bar{W} = c_w \frac{e_1}{E} \left(\frac{\Delta K_1^2}{R_0^{2(1-\lambda_1)}} \right) \quad (15)$$

It is worth of mentioning that the application of the SED criterion and the reliability of its results are strictly related to the proper determination of fatigue parameters, i.e. the critical value of deformation energy and the radius of the control volume. The control radius R_0 , can be easily estimated by means of the following expression:

$$R_0 = \left(\frac{\sqrt{2e_1} \Delta K_{1A}}{\Delta \sigma_A} \right)^{\frac{1}{1-\lambda_1}} \quad (16)$$

where ΔK_{1A} and $\Delta \sigma_A$ are the reference values at high cycle fatigue of the notch stress intensity factor range of the severely notched material and the nominal stress range of the unnotched material, respectively. As soon as the notch stress intensity factor ΔK_{1A} is known, the control radius can be evaluated. Due to the lack of data of the critical stress intensity factors for different materials an alternative procedure is suggested here to evaluate R_0 .

An alternative approach for the evaluation of R_0 is proposed here. By referring to the fatigue strength of plain and notched samples at N_A cycles, which is the reference value of number of cycles to failure in the high-cycle fatigue regime, the value of R_0 can be obtained by equating the strain

energy density of the unnotched sample to the averaged strain energy density over the sector of radius R_0 surrounding the tip of the notch as shown in Eq. (17):

$$\Delta\bar{W}_0^{\text{plain}} = \frac{\sigma_{A,p}^2}{2E} = \Delta\bar{W}^{\text{notch}}(R_0) \quad (17)$$

$\sigma_{A,p}$ is the fatigue strength of the smooth sample at N_A cycles and E is the elastic modulus of the material. Fig. 4 shows the procedure for the evaluation of the control radius R_0 of the critical volume by using linear elastic FEA. By varying the control radius R around the notch tip in the FE model under a nominal stress $\sigma_{A,n}$, the corresponding values of the strain energy density value $\Delta\bar{W}^{\text{notch}}$ averaged over the control volume can be easily evaluated. It is then possible to fit $\Delta\bar{W}^{\text{notch}}(R)$ as a function of the control radius R obtaining a fitting equation. The control radius R_0 can be calculated by equating $\Delta\bar{W}^{\text{notch}}(R)$ to the strain density energy from the plain samples, $\Delta\bar{W}_0^{\text{plain}}$. Due to the lack of experiments providing the critical values of the stress intensity factors, the control radius can be easily evaluated with the procedure explained above.

The local SED can also be easily and directly calculated from the post-processing of the FEA by summing the energy contributions $W_{\text{element},i}$ for all the finite element within the control volume V :

$$\Delta\bar{W} = c_w \frac{\sum_v W_{\text{element},i}}{V} \quad (18)$$

The parameter c_w of Eq. (18) takes into account the load ratio R when the nominal stress amplitude is applied to the FE model to obtain the local SED value [60]. As previously mentioned it is important to remember that refined mesh are not necessary to determine the values of the SED, because this parameter can be determined via the nodal displacements, without involving their derivatives [61]. This means that the mean value of the local SED is substantially independent of the mesh size. The value of the SED in the control volume can be accurately determined through FEA using regular coarse meshes.

It should be mentioned that the assumption of the SED as a damage parameter allows to summarize a lot of fatigue data obtained for notched specimens in a reasonable scatter band. Generally, it is important to understand the fatigue behavior of notched components and to assess with a reasonable accuracy the fatigue strength without performing a large number of experiments. Therefore, in order to predict the fatigue life of components having different geometrical features,

the SED $\overline{\Delta W}$ versus the fatigue life N_f relationship is calculated by considering the notched samples as sharp as possible following the same approach developed for the TCD and described above. In complete analogy with the process employed for the TCD by applying in the FE model a value of nominal stress, the averaged SED, $\overline{\Delta W}$, can be evaluated from the post-processing of the FE results by employing Eq. (18). $\overline{\Delta W}$ versus the number of cycles to failure N_f can be expressed as follows:

$$\overline{\Delta W} = C \cdot N_f^D \quad (19)$$

In Eq. (19) C and D are material constants. Keeping constant the material and the nominal load ratio, the fatigue life can be assessed by using Eq. (19) for any geometrical configuration of the notch. The flow-chart summarizing the procedure used to estimate fatigue lifetime is shown in Fig.5.

2.3 TCD Method validation by experimental data

In order to validate the accuracy of the TCD in predicting the fatigue life of notched components, some data sets taken from the literature have been re-analyzed in the present investigation. The selected series of data under uniaxial loading are listed in Table 1. For the selected series the nominal load ratio varies from -1 up to 0.5. It is worth mentioning that the constants A and B in Eq.(4) have been determined by considering the fatigue curve corresponding to unnotched material and that from very sharp notches (i.e. the highest value of the stress concentration factor).

The accuracy of the TCD approach in predicting the number of cycles to failure as a function of different geometrical configuration is summarized by the diagrams reported in Fig. 6. Point and line methods have been applied here to summarize the data. In Fig. 6 the experimental number of cycles to failure, N_f , are plotted against the estimated number of cycles to failure, $N_{f,e}$. The scatter bands have been calculated by considering the fatigue data from plain specimens and from the sharpest notched configuration available for each set of data. A probability of survival, P_s , equal to 5% and 95%, has been considered. The results summarized in Fig. 6 confirm that the TCD method is successful in predicting the uniaxial fatigue behavior of different materials. All the data, in fact, fall within the scatter band of the parent material with the only exception of the samples characterized by a lower value of the stress concentration factor. When the stress concentration factor (K_t) decreases, the final fatigue assessment tend to be too conservative. On the other hand the prediction of the data characterized by a higher value of K_t always fall within the scatter band, showing a high accuracy

in the final assessment of the fatigue life. In general, the overall best accuracy is achieved by applying the LM, whereas the application of the PM results in slightly conservative predictions.

2.4 SED Method validation by experimental data

The synthesis of the same original experimental data in terms of averaged SED has been performed in the present section of the paper. All the main parameters necessary to apply the SED approach are summarized in Table 2. The relationship linking the local SED with N_f , the stress-based scatter index T_σ , the strain energy-based scatter index T_w referred to a probability of survival in the range of 10%-90% and the control radius R_0 are summarized in Table 2 for each material. It can be noted that the value of T_w becomes equal to the value of T_σ when reconverted to an equivalent local stress range ($T_\sigma = \sqrt{T_w}$).

The SED accuracy in the fatigue prediction has been validated in Fig. 7. The results reported in Fig. 7 confirm that the SED method is able to predict with good accuracy the fatigue data from different materials and geometries with all the data falling within the scatter band of the parent material with the only exception of the notched specimens characterized by a low value of the stress concentration factor.

In order to precise comparison of the calculation results obtained with the discussed methods, the methods prediction error can be defined according to the following relationship [65, 66]:

$$E_N = \log_{10} \left(\frac{N_f}{N_{f,e}} \right) \quad (20)$$

The probability density function of errors of fatigue life determination is shown in Fig. 8, which shows the similar distribution as shown in Figs. 6 and 7. From the figure it appears that the errors are slightly displaced towards the safe area for the results calculated by the TCD, but the errors by the SED are sometimes unsafe and other times safe without a clear regularity.

3 Fatigue assessment of unnotched and notched components under multiaxial fatigue loading

3.1 The MWCM in fatigue assessment

Several multiaxial fatigue criteria have been formalized and validated in order to make reliable and accurate fatigue predictions of components subjected to complex multiaxial loading paths. Among these different criteria, the Critical Plane Method based criteria have been found very effective [67-70]. In particular the Modified Wöhler Curve Method (MWCM) has been successfully

applied not only to unnotched specimens but also to notched components subjected to different multiaxial loading conditions [71-73].

The MWCM postulates that the fatigue damage mainly depends on the maximum shear stress amplitude τ_a , the mean value $\sigma_{n,m}$ and the amplitude of the normal stress $\sigma_{n,a}$ measured on the critical plane [71, 73, 74]. The effective value of the critical plane stress ratio, ρ_{eff} , can be defined as follows:

$$\rho_{\text{eff}} = \frac{m\sigma_{n,m} + \sigma_{n,a}}{\tau_a} \quad (21)$$

In Eq. (21) m is the mean stress sensitivity index, which is a material constant ranging between 0 and 1. It gives a measure of the material sensitivity to nonzero mean stresses perpendicular to the critical planes. In particular, m takes on the following value:

$$m = \frac{\tau_a^*}{\sigma_{n,m}^*} \left(2 \frac{\tau_0 - \tau_a^*}{2\tau_0 - \sigma_0} - \frac{\sigma_{n,a}^*}{\tau_a^*} \right) \quad (22)$$

where τ_a^* , $\sigma_{n,m}^*$ and $\sigma_{n,a}^*$ are the critical plane stress components determined under a load ratio, R , larger than -1, where the relevant stress components relative to the critical plane. σ_0 and τ_0 are fully reversed uniaxial fatigue limit and fully reversed torsional fatigue limit, respectively. In general, when the mean stress sensitivity index m is not available, the material can be assumed to be fully sensitive to the presence of non-zero mean stresses perpendicular to the critical planes (i.e., $m=1$), increasing the degree of conservatism of the estimates [30].

A large amount of experimental data have shown that the fatigue lifetime can be estimated through the degree of multiaxiality of the stress field damaging the fatigue process zone in terms of ρ_{eff} [30, 72]. According to the modified Wöhler diagrams, the negative inverse slope, $k_\tau(\rho_{\text{eff}})$ versus ρ_{eff} and the reference shear stress amplitude, $\tau_{A,\text{Ref}}(\rho_{\text{eff}})$ versus ρ_{eff} relationships are obtained by running appropriate experiments as shown in Fig. 9. The calibration functions are defined as follow:

$$k_\tau(\rho_{\text{eff}}) = a\rho_{\text{eff}} + b \quad (23)$$

$$\tau_{A,\text{Ref}}(\rho_{\text{eff}}) = \alpha\rho_{\text{eff}} + \beta \quad (24)$$

where a , b , α and β are fatigue constants to be determined experimentally. The accuracy of constants can be increased by considering a large number of fatigue curves for the calibration.

Fig. 9 summarizes the use of the MWCM method to estimate the fatigue lifetime of components. In more detail, from the stress state at point O, the maximum shear stress amplitude, τ_a , and the effective critical plane stress ratio, ρ_{eff} , can be determined by taking full advantage of the Maximum

Variance Methods [75-78]. The Maximum Variance Method assumes that the fatigue damage is proportional to the variance of the load history that is damaging, at the assumed critical point, the component being assessed. Subsequently, according to the calculated value of ρ_{eff} , the modified Wöhler curve corresponding to the degree of multiaxiality of the considered stress field acting on the fatigue process zone can be estimated directly from Eqs (23) and (24). In general, when the degree of multiaxiality of the stress field relative to the fatigue process zone is evaluated in terms of ρ_{eff} , the constants of functions $k_{\tau}(\rho_{\text{eff}})$ and $\tau_{A,\text{Ref}}(\rho_{\text{eff}})$ have to be determined by using the fully reversed uniaxial and torsional fatigue curves. Finally, fatigue lifetime of plain components under the investigated loading condition can be predicted by using the following equation:

$$N_{f,e} = N_0 \left[\frac{\tau_{A,\text{Ref}}(\rho_{\text{eff}})}{\tau_a} \right]^{k_{\tau}(\rho_{\text{eff}})} \quad (25)$$

In the light of the good accuracy shown by the TCD when employed to predict fatigue lifetime of notched components, the extension of MWCM has been also proposed to be applied in terms of the TCD to predict the fatigue lifetime of notched components. It is worth noting that among the different formalizations of the TCD, PM has been used to estimate high-cycles fatigue strength because the stress state at one single point is much easier to be handled under complex multiaxial load histories. As postulated by the TCD, the critical distance value to be used to calculate an effective equivalent stress is a material dependent property whose value increases with decreasing the number of cycles to failure as shown in Eq. (4).

To estimate the fatigue life, the employed methodology is described in Fig. 10. In more detail, initially the linear-elastic stress distribution along the focus path r has to be calculated by using either analytical or numerical methods. The values of the effective value of the critical plane stress ratio, $\rho_{\text{eff}}(r)$, the maximum shear stress amplitude, $\tau_a(r)$, the amplitude of the stress perpendicular to the critical plane, $\sigma_{n,a}(r)$ and the mean stress perpendicular to the critical plane, $\sigma_{n,m}(r)$, are calculated at the critical plane identified along the focus path, as shown in Fig. 10. At any distance r from the notch tip, and according to the calculated values of τ_a and ρ_{eff} , the corresponding modified Wöhler curve can be estimated by using the k_{τ} vs. ρ_{eff} and $\tau_{A,\text{Ref}}$ vs. ρ_{eff} relationships previously calibrated through the parent material fatigue properties. The corresponding number of cycles to failure, N_f can be calculated directly at any point belonging to the focus path. Subsequently, for any value of r , the critical distance L_M is calculated according to Eq. (4). Finally, the component to be assessed is assumed to fail at the number of cycles to failure, $N_{f,e}$, when the distance r is equal to the critical

distance $L_M/2$, that is:

$$\frac{L_M}{2} - r = 0 \Rightarrow \frac{A \cdot N_{f,e}^B}{2} - r = 0 \quad (26)$$

3.2 Multiaxial fatigue assessment by means of SED

Ellyin et al. suggested that fatigue life of unnotched components can be made by considering both the plastic energy and the positive elastic energy [40, 41]. This assumption is based on the experimental evidence that, in the high-cycle fatigue regime fatigue damage mainly depends on the contribution of elastic energy due to the plastic energy is in general negligible [79].

The elastic strain increment is related to the stress increment through the generalized Hooke's law:

$$d\varepsilon_{ij}^e = \frac{1+\nu}{E} \sigma_{ij} - \frac{\nu}{E} d\sigma_{kk} \delta_{ij} \quad (27)$$

In Eq. (27) ν is the Poisson ratio, E the Young modulus and δ_{ij} the Kronecker delta. δ_{ij} is equal to 1 when $i=j$ and it is equal to 0 otherwise, and a repeated index implies summation over its range, $\sigma_{kk} = \sigma_{11} + \sigma_{22} + \sigma_{33}$, in this case $i, j=1, 2, 3$.

The elastic SED can be calculated as,

$$W = \int \sigma_{ij} d\varepsilon_{ij}^e \quad (28)$$

For an isotropic linear elastic material, by substituting Eq. (27) into Eq. (28) and integrating the following expression can be obtained:

$$\Delta W = \frac{1+\nu}{2E} S_{ij} S_{ij} + \frac{1-2\nu}{6E} (\sigma_{kk})^2 \quad (29)$$

The first term on the right hand side of the equation is the deviatoric strain energy density, while the second term is related to the strain energy linked to the volume change. The following expressions can then be written:

$$J_2 = \frac{1}{3} [I_1^2 + 3I_2] \quad (30)$$

In Eq. (30) $I_1 = \sigma_{xx} + \sigma_{yy} + \sigma_{zz}$ and $I_2 = -(\sigma_{xx}\sigma_{yy} + \sigma_{yy}\sigma_{zz} + \sigma_{xx}\sigma_{zz}) + (\tau_{xy}^2 + \tau_{yz}^2 + \tau_{zx}^2)$ are the first and second invariants of the stress tensor, respectively.

By using the above relationships, it is straightforward to obtain ΔW_e for plain specimens under multiaxial fatigue loading:

$$\Delta W = \frac{\Delta \sigma_{\text{nom}}^2}{2E} + (1 + \nu) \frac{\Delta \tau_{\text{nom}}^2}{E} \quad (31)$$

With the aim to unify in a single diagram the fatigue data related to different values of the nominal load ratio R , it is also necessary to consider a weighting factor in the the previous expression. For unnotched specimens under different loading modes, substituting from Eq. (14) into Eq. (31), the expressions become:

$$\Delta W_e = c_w \left(\frac{\Delta \sigma_{\text{nom}}^2}{2E} + (1 + \nu) \frac{\Delta \tau_{\text{nom}}^2}{E} \right) \quad (32)$$

As shown in the first part of the paper, the SED as a damage parameter allows all the fatigue data obtained from plain specimens with different loading modes to be summarized in a narrow scatterband. $\overline{\Delta W}$ versus the fatigue life N_f can be expressed as follows, in analogy with the Wöhler curve representation:

$$\overline{\Delta W} = A \cdot N_f^B \quad (33)$$

In Eq. (33) A and B are material constants. As soon as the curve $\overline{\Delta W} - N_f$ is drawn, Eq. (33) is very convenient to determine the different values of $\overline{\Delta W}$ as a function of the fatigue life N_f .

The extension to notched components is more complicated due to the effects of the stress concentration and stress gradients in the proximity of the notch tip. The notch stress field is dependent on the notch shape and its dimensional features. For structural components subjected to multiaxial loading conditions in presence of V-notches with a small root radius mode I and mode III NSIFs, K_1 and K_3 , can quantify the stress field in the vicinity of the notch tip [53]. The averaged strain energy calculation is based on the local stress and strain state in a control volume embracing the notch tip. These parameters are evaluated from linear elastic FE analyses taking into consideration a sharp V-notch with tip radius equal to 0 (see Fig. 11). In particular, with reference to the coordinate system shown in Fig. 11, the mode I and mode III NSIFs can be defined by means of the following expressions [80-82]:

$$K_1 = \sqrt{2\pi} \lim_{r \rightarrow 0^+} r^{1-\lambda_1} \sigma_{\theta\theta} (r, \theta = 0) \quad (34)$$

$$K_3 = \sqrt{2\pi} \lim_{r \rightarrow 0^+} r^{1-\lambda_3} \tau_{r\theta} (r, \theta = 0) \quad (35)$$

The eigenvalues λ_1 and λ_3 depend on the notch opening angle 2α . On the other hand, in conditions of linear elastic hypothesis, the NSIFs can be linked to the nominal stress components

according to the following expressions [60, 81]:

$$\Delta K_1 = k_1 d^{1-\lambda_1} \Delta \sigma_{\text{nom}} \quad (36)$$

$$\Delta K_3 = k_3 d^{1-\lambda_3} \Delta \tau_{\text{nom}} \quad (37)$$

where d is the notch depth, while k_1 and k_3 are non-dimensional factors derived from FE analyses, which simply take into account the shape of the component, in analogy with the representation of linear elastic fracture mechanics. In the case of V-notched specimens subjected to mode I+III under linear elasticity hypothesis, the SED averaged over a control volume, which embraces the notch tip, can be expressed by means of the following equation [83]:

$$\Delta \bar{W} = \frac{1}{E} \left[e_1 \cdot \frac{\Delta K_1^2}{R_1^{2(1-\lambda_1)}} + e_3 \cdot \frac{\Delta K_3^2}{R_3^{2(1-\lambda_3)}} \right] \quad (38)$$

In Eq. (38) ΔK_1 and ΔK_3 represent the values of Mode I and Mode III NSIF ranges, while R_1 and R_3 are the radius of the control volume under Mode I and Mode III. The functions e_1 and e_3 are two parameters related to the V-notch geometry. These parameters are directly linked to the integrals of the angular functions over the control volume of tip and can be determined once the V-notch opening angle is known [46, 54].

The calculation of NSIFS requires a refined mesh in the proximity of the notch tip where the stress field is singular. On the other hand, the SED averaged over a control volume can be accurately obtained by means of relatively coarse meshes as explained in previous works [14]. By considering independently Mode I and Mode III loading, the control radii R_1 and R_3 can be estimated. They can be estimated by considering the high-cycle fatigue strengths derived from unnotched specimens and the values of ΔK_{1A} and ΔK_{3A} referred to a number of cycles N_A , belonging to the high-cycle fatigue regime:

$$R_1 = \left(\sqrt{2e_1} \cdot \frac{\Delta K_{1A}}{\Delta \sigma_{1A}} \right)^{\frac{1}{1-\lambda_1}} \quad (39)$$

$$R_3 = \left(\sqrt{\frac{e_3}{1+\nu}} \cdot \frac{\Delta K_{3A}}{\Delta \tau_{3A}} \right)^{\frac{1}{1-\lambda_3}} \quad (40)$$

In order to unify in a common diagram the fatigue results by adopting different nominal load ratio R , the weighting parameter c_w has to be taken into account. Therefore, the final expression becomes as follow:

$$\text{SED} = c_w \times \Delta \bar{W} = \frac{c_w}{E} \left[e_1 \times \frac{\Delta K_1^2}{R_1^{2(1-\lambda_1)}} + e_3 \times \frac{\Delta K_3^2}{R_3^{2(1-\lambda_3)}} \right] \quad (41)$$

When blunt notches are considered, the application of NSIFs is not longer valid. In this case, the averaged SED can be linked to the elastic peak stress at the notch tip. The total strain energy density, calculated at the notch tip, can be expressed as [52, 53]:

$$\Delta W = \frac{c_w}{2E} \left[\Delta \sigma_{p,el}^2 + 2(1+\nu) \Delta \tau_{p,el}^2 \right] \quad (42)$$

In Eq. (42) E and ν are the Young modulus and the Poisson ratio, and $\Delta \sigma_{p,el}$ and $\Delta \tau_{p,el}$ are the elastic peak stress ranges at the notch tip. Eq. (42) can be also rewritten in terms of the theoretical stress concentration factors:

$$\Delta W = \frac{c_w}{2E} \left[K_{t,net,axial}^2 \Delta \sigma_{net}^2 + 2(1+\nu) K_{t,net,torsional}^2 \Delta \tau_{net}^2 \right] \quad (43)$$

As previously made in the paper $\Delta \bar{W}$ can be related to N_f by means of the following expression:

$$\Delta \bar{W} = C N_f^D \quad (44)$$

where C and D are material constants. The fatigue life can be assessed by using Eq. (44) for notched components under multiaxial loading.

3.3 MWCM method validation by using unnotched components

The systematic validation of the proposed method was performed by using a large number of experimental data taken from the literature. A synthesis is provided in Table. 3 where the constants of the two fatigue master curves used to calibrate the method were reported together with the fully reversed fatigue limits σ_A and τ_A , the ultimate strength σ_u and reference number of cycles to failure N_A .

In order to get a good understanding of the statistical distribution by using the MWCM, Fig. 12 shows the correlation of experimental fatigue life N_f versus estimated fatigue life $N_{f,e}$ for all the materials re-analyzed in the present work. In these diagrams, both multiaxial fatigue data and calibration data are plotted together. Calibration data include the uniaxial, bending and torsional data used to calibrate by means of Eqs (23) and (24) the MWCM criterion. In the diagrams, the continuous straight lines define the uniaxial or bending scatter bands, while the dashed lines define the torsional scatter bands. As mentioned above, all scatter bands were calculated under the hypothesis of a log-normal distribution of the number of cycles to failure, with a confidence level equal to 95%.

Fig. 12 shows that all data from multiaxial specimens mainly fall within the widest scatter band related either to uniaxial or to torsional loadings. This simply means that the MWCM allows a sound multiaxial fatigue life prediction characterized by a statistical scatter index close to those exhibited by the two master curves used to calibrate the method. The intrinsic dispersion of the two calibration curves obviously influences the degree of accuracy of the predictions under multiaxial fatigue conditions. More precise predictions can only be obtained by reducing the dispersion of data belonging to the master curves keeping into consideration additional parameters.

In the majority of the cases the effect of the mean value of the torsional stress can be disregarded, but this does not hold true, for example, in the case of 18G2A steel specimens as shown in Fig. 12. This material is very sensitive to the mean value of the torsional component and this causes non-conservative fatigue lifetime predictions when the load ratio R is larger than -1 . Conservative predictions in the fatigue life have been observed for low carbon steel. This over conservative estimations can be explained considering that this material tends to have non negligible plastic deformation also in the high cycle fatigue regime.

3.4 SED validation under multiaxial loading

The synthesis of the original experimental data in terms of the SED method according to Eq. (32) has been evaluated. All the data for a suitable application of the criterion are listed in Table 4. The scatter index values are close to those previously suggested by Haibach. The SED accuracy in the case of multiaxial loading conditions is well visible in Fig. 13, which reported the experimental number of cycles to failure, N_f , versus the estimated number of cycles to failure, $N_{f,e}$. In particular, the continuous straight lines define the uniaxial scatter bands, while the dashed lines define the torsional scatter bands, by post-processing the experimental data generated by testing plain specimens under both uniaxial and torsional fully-reversed loading. The probability density function of calculation errors, shown in Fig. 14, proves the accuracy of predicting results obtained from the two models. The obtained results calculated by the SED are mostly in the same proportion at the safe and dangerous sides.

The diagrams in Fig. 13 make it evident that the systematic adoption of Eq. (32) resulted in estimating fatigue life mainly falling within the parent material torsional scatter band for the majority of the considered materials. These diagrams clearly show that the SED is an accurate method for a wide variety of multiaxial loading configurations. The SED method summarises all the experiment

data under different loading condition together to get the SED $\Delta\bar{W}$ versus the fatigue life N_f relationship through a least squares linear regression. Its main advantage is that the best fitting line is the line with minimum error from all the points, which could correct the error efficiently. Therefore, in order to predict the fatigue life of plain specimens, the SED $\Delta\bar{W}$ versus the fatigue life N_f relationship is calculated accurately by a large number of fatigue experimental data.

The only effect on this in the prediction is that the SED is not able to take into account the effect of non proportional loading that for many materials is negligible. So this is not a drawback in many cases. In addition, as a scalar quantity within a volume, the SED method cannot consider the preferential orientation of crack path. The assumption might be acceptable from an engineering point of view only considering the crack initiation life, and not the whole fatigue life of the component, which is also a limitation of the TCD.

3.5 MWCM validation using notched components

In order to investigate the accuracy of the MWCM applied in conjunction with the PM, some multiaxial fatigue data results taken from the literature. According to the procedure briefly explained above, the two fatigue curves generated by testing, under full-reversed uniaxial fatigue loading, the plain specimens and the notched samples, respectively, have been used to calculate constants A and B in the L_M versus N_f relationship. The constants a , b , α and β as well as ρ_{lim} have been determined through the uniaxial and torsional fully reversed plain fatigue curves. The mean stress sensitivity index, m , has been estimated by using a uniaxial limit generated under a load ratio, R , larger than -1. The values of the constants needed to calibrate both the MWCM and the L_M versus N_f relationship are summarized in Table 5.

The N_f versus $N_{f,e}$ diagrams reported in Fig. 15 are able to prove that the MWCM method is successful in estimating the lifetime of notched components under multiaxial loading. In particular, these results confirm that MWCM is capable of making the estimates located mainly within the widest plain scatter band between the two used to calibrate. Fig. 15 also clearly proves that MWCM in terms of PM can be highly accurate in predicting fatigue life, correctly taking into account not only the presence of various stress concentration factors derived from notches but also the damaging effect of stress gradients due to the nominal loading. Moreover, it has to be said that, strictly speaking, the constants of the L_M versus N_f relationship under torsion is different from these values determined under uniaxial fatigue loading. The critical distance value under torsion is larger than the

corresponding value determined under uniaxial fatigue loading [84]. By reanalyzing large amount of experimental data, the results strongly support the validity of the idea that the L_M versus N_f relationship generated under uniaxial fatigue loading can be assumed to be independent of the complexity of the assessed stress field. But for some materials, like Ti6Al4V and 39NiCrMo3 in Fig. 15, the predicting results show that the pure torsional data fall outside the widest parent material scatter band and tend to conservative lifetime prediction, with loss of accuracy. It is important to highlight that under pure torsional loading there are a large plastic zone ahead of the notch tip for V-notch Ti6Al4V and 39NiCrMo3 specimens [56, 57]. Therefore, the predicting fatigue life under pure torsion loading would be conservative if the L_M versus N_f relationship generated under uniaxial fatigue loading was used to calculate the fatigue life.

3.6 The SED method validation by using notched components

The multiaxial fatigue behavior of materials under different loading conditions has been investigated to analyze the influence of load ratio and load phase angle on the fatigue life of specimens weakened by notches with different root radius. Synthesis of the experimental results taken from the literature is shown in Table 6 together with the main parameters necessary for the application of the SED approach. It is observed that the scatter index T_σ and T_w are quite narrow, with a probability of survival of 10-90%. In terms of equivalent stress range (by simply making the square root of scatter index T_w), the scatter index results are nearly equal to the Haibach scatter band T_σ . Under linear elastic hypothesis, the contribution ascribable to the stress component $\Delta\sigma$ has been averaged over a control radius R_1 , while the ascribable to the stress component $\Delta\tau$ has been averaged over a control radius R_3 . The later radius definition is strongly influenced by extrinsic mechanism summarized by the term crack tip shielding (plasticity, rough contact surface and corrosion debris). In the present investigation, as dealing with high notch sensitivity of notched specimens, plasticity and shielding effects are very limited and play only a second role on the fatigue crack initiation and propagation. Therefore, a single control radius can also be used to obtain satisfied results without considering the loading modes [52]. For large radius of blunt V and U notched specimens, “the point criterion” based on the SED method at the notch tip is adopted to calculate the data.

Finally, Fig. 16 reports the experimental number of cycles to failure, N_f , versus the estimated number of cycles to failure, $N_{f,e}$. It is important to highlight that in such diagrams not only the experimental data but also the scatter bands of the calibration fatigue curves plotted, including the

torsional scatter bands and the uniaxial scatter bands of parent materials. These scatter bands refer to a probability of survival, P_s , equal to 5 and 95%, respectively. These results confirm that the method is giving fatigue predictions mainly falling within the uniaxial scatter band or the torsional scatter band, which can also be proved by the course of the probability density function as shown in Fig. 17. When the errors are calculated for the MWCM, the results are not located around the mean error equal to zero. Compared with the MWCM, the obtained results by SED are nearly in the same proportion at the safe and dangerous sides. Although the re-analysis of the experimental data in terms of the SED range at the notch tip allows most of the uniaxial and multiaxial data referred to notched specimens to be summarized in the fatigue scatter band, there are still some data falling outside the largest scatter bands. A possible explanation might involve the different influence that tensile and torsion loads have on the local yielding in the highly stressed regions [56]. It is extensive plasticity provoked by torsion loading with nonlinear effects and by interference phenomena between the crack surfaces. Moreover, the proposed procedure shows that the SED approaches need large amount of fatigue data to obtain high accuracy and reliability of predicting fatigue life, which might be complex and high cost from an engineering point of view.

4 Conclusions

(1) The TCD approach can successfully assess the fatigue life of notched components subjected to uniaxial loading, and it held true independently of the geometrical feature weakening the tested specimens. The TCD approach in the line method has been found to be more accurate than the point method in assessing the fatigue lifetime of notched specimens.

(2) The SED approach has been also found to be an accurate design methodology under uniaxial loading, with exception to U notches with low stress concentration factors. The approach is very sensitive to the critical radius value, which defines the control area. The critical radius can be easily estimated using the appropriate equation depending on the fatigue strength of plain specimens and the notch stress intensity factor at a specific reference number of cycles.

(3) The MWCM itself and its combination with the point method has been found to be highly accurate in estimating the multiaxial fatigue lifetime of plain and notched components. The method can be easily implemented to assess the lifetime of real structures by means of a simple linear elastic FEA. Under torsional loading, the mean stress has obvious effect on the accuracy of predicted fatigue life. For some materials, due to the presence of a large plastic zone surrounding the crack tip, the application of TCD constants obtained from uniaxial loading to torsional loading can yield to

inaccurate results. This is due to the different stress field distribution in these two loading cases and their different effects on the plastic zone.

(4) The SED has highly accuracy in assessing the fatigue lifetime of plain and notched components under multiaxial loading. Using the averaged SED, the reanalysis of the data on different volumes allows to summarise the main body of the results in a single, narrow scatter band relative to the fatigue results of parent materials generated under torsional or uniaxial loading.

Acknowledgement

The authors would like to acknowledge the support by the Innovation Program (237099000000170004) and the State Key Laboratory Program (614221305020617) and also by the China Scholarship Council (Grant No. 201705290009).

Reference

- [1] A. Fatemi, N. Shamsaei, Multiaxial fatigue: An overview and some approximation models for life estimation, *Int J Fatigue*, 33 (2011) 948-958.
- [2] A. Carpinteri, A. Spagnoli, Multiaxial high-cycle fatigue criterion for hard metals, *Int J Fatigue*, 23 (2001) 135-145.
- [3] A. Fatemi, D.F. Socie, A critical plane approach to multiaxial fatigue damage including out-of-phase loading, *Fatigue Fract Eng M*, 11 (1988) 149-165.
- [4] P. Luo, W. Yao, L. Susmel, Y. Wang, X. Ma, A survey on multiaxial fatigue damage parameters under non-proportional loadings, *Fatigue Fract Eng M*, 40 (2017) 1323-1342.
- [5] D. Taylor, The theory of critical distances, *Eng Fract Mech*, 75 (2008) 1696-1705.
- [6] L. Susmel, The theory of critical distances: a review of its applications in fatigue, *Eng Fract Mech*, 75 (2008) 1706-1724.
- [7] L. Susmel, D. Taylor, The Theory of Critical Distances to estimate lifetime of notched components subjected to variable amplitude uniaxial fatigue loading, *Int J Fatigue*, 33 (2011) 900-911.
- [8] L. Susmel, R. Tovo, Estimating fatigue damage under variable amplitude multiaxial fatigue loading, *Fatigue Fract Eng M*, 34 (2011) 1053-1077.
- [9] A.A. Ahmed, L. Susmel, A material length scale based methodology to assess static strength of notched additively manufactured polylactide (PLA), *Fatigue Fract Eng M*, 41 (2018) 2071-2098.
- [10] R. Wang, H. Liu, D. Hu, D. Li, J. Mao, Evaluation of notch size effect on LCF life of TA19 specimens based on the stress gradient modified critical distance method, *Fatigue Fract Eng M*, 41 (2018) 1794-1809.
- [11] P. Lazzarin, F. Berto, Some Expressions for the Strain Energy in a Finite Volume Surrounding the Root of Blunt V-notches, *Int J Fracture*, 135 (2005) 161-185.
- [12] P. Livieri, P. Lazzarin, Fatigue strength of steel and aluminium welded joints based on generalised stress intensity factors and local strain energy values, *Int J Fracture*, 133 (2005) 247-276.
- [13] F. Berto, P. Lazzarin, A review of the volume-based strain energy density approach applied to V-notches and welded structures, *Theor Appl Fract Mec*, 52 (2009) 183-194.
- [14] F. Berto, P. Lazzarin, Recent developments in brittle and quasi-brittle failure assessment of engineering materials by means of local approaches, *Materials Science and Engineering: R: Reports*, 75 (2014) 1-48.
- [15] F. Berto, P. Lazzarin, Fatigue strength of Al7075 notched plates based on the local SED averaged over a control volume, *Sci. China. Phys. Mech.*, 57 (2014) 30-38.
- [16] W. Song, X. Liu, F. Berto, P. Wang, H. Fang, Fatigue failure transition analysis in load-carrying

- cruciform welded joints based on strain energy density approach, *Fatigue Fract Eng M*, 40 (2017) 1164-1177.
- [17] S.P. Zhu, Y. Liu, Q. Liu, Z.Y. Yu, Strain energy gradient-based LCF life prediction of turbine discs using critical distance concept, *Int J Fatigue*, 113 (2018) 33-42.
- [18] S.P. Zhu, Z.Y. Yu, Q. Liu, I. Ayhan, Strain energy-based multiaxial fatigue life prediction under normal/shear stress interaction, *International Journal of Damage Mechanics*, in press, doi: 10.1177/1056789518786031.
- [19] H. Neuber, *Theory of notch stresses*, Springer-Verlag, Berlin, (1958).
- [20] R.E. Peterson, Notch sensitivity, *Metal fatigue*, (1959) 293-306.
- [21] K. Tanaka, Engineering formulae for fatigue strength reduction due to crack-like notches, *Int J Fracture*, 22 (1983) R39-R46.
- [22] P. Lazzarin, R. Tovo, G. Meneghetti, Fatigue crack initiation and propagation phases near notches in metals with low notch sensitivity, *Int J Fatigue*, 19 (1997) 647-657.
- [23] D. Taylor, Geometrical effects in fatigue: a unifying theoretical model, *Int J Fatigue*, 21 (1999) 413-420.
- [24] M. El Haddad, T. Topper, K. Smith, Prediction of non propagating cracks, *Eng Fract Mech*, 11 (1979) 573-584.
- [25] L. Susmel, D. Taylor, A novel formulation of the theory of critical distances to estimate lifetime of notched components in the medium - cycle fatigue regime, *Fatigue Fract Eng M*, 30 (2007) 567-581.
- [26] L. Susmel, D. Taylor, On the use of the Theory of Critical Distances to predict static failures in ductile metallic materials containing different geometrical features, *Eng Fract Mech*, 75 (2008) 4410-4421.
- [27] D. Taylor, The Theory of Critical Distances: A link to micromechanisms, *Theor Appl Fract Mec*, 90 (2017) 228-233.
- [28] L. Susmel, D. Taylor, A critical distance/plane method to estimate finite life of notched components under variable amplitude uniaxial/multiaxial fatigue loading, *Int J Fatigue*, 38 (2012) 7-24.
- [29] L. Susmel, D. Taylor, The theory of critical distances to estimate finite lifetime of notched components subjected to constant and variable amplitude torsional loading, *Eng Fract Mech*, 98 (2013) 64-79.
- [30] L. Susmel, D. Taylor, The Modified Wöhler Curve Method applied along with the Theory of Critical Distances to estimate finite life of notched components subjected to complex multiaxial loading paths, *Fatigue Fract Eng M*, 31 (2008) 1047-1064.
- [31] G. Sih, *A Special Theory of Crack Propagation: Methods of Analysis and Solutions of Crack*

- Problems, Mechanics of Fracture I, ed. GC Sih, in, Noordhoff International Publishing, Leyden, 21, 1973.
- [32] G.C. Sih, Strain-energy-density factor applied to mixed mode crack problems, *Int J Fracture*, 10 (1974) 305-321.
- [33] M. Kipp, G. Sih, The strain energy density failure criterion applied to notched elastic solids, *Int J Solids Struct*, 11 (1975) 153-173.
- [34] G.C. Sih, *Mechanics of fracture initiation and propagation: surface and volume energy density applied as failure criterion*, Springer Science & Business Media, 2012.
- [35] G. Sih, J. Ho, Sharp notch fracture strength characterized by critical energy density, *Theor Appl Fract Mec*, 16 (1991) 179-214.
- [36] L.F. Gillemot, Criterion of crack initiation and spreading, *Eng Fract Mech*, 8 (1976) 239-253.
- [37] F. Gillemot, E. Czoboly, I. Havas, Fracture mechanics applications of absorbed specific fracture energy: notch and unnotched specimens, *Theor Appl Fract Mec*, 4 (1985) 39-45.
- [38] G. Glinka, Energy density approach to calculation of inelastic strain-stress near notches and cracks, *Eng Fract Mech*, 22 (1985) 485-508.
- [39] G. Sih, C. Chao, Failure initiation in unnotched specimens subjected to monotonic and cyclic loading, *Theor Appl Fract Mec*, 2 (1984) 67-73.
- [40] F. Ellyin, Cyclic strain energy density as a criterion for multiaxial fatigue failure, in: *ICBMFF2*, 1985.
- [41] F. Ellyin, K. Golos, Multiaxial fatigue damage criterion, *J. Eng. Mater. Technol.*, 110 (1988) 63-68.
- [42] K. Molski, G. Glinka, A method of elastic-plastic stress and strain calculation at a notch root, *Materials Science and Engineering*, 50 (1981) 93-100.
- [43] F. Ellyin, *Fatigue damage, crack growth and life prediction*, Springer Science & Business Media, 2012.
- [44] F. Ellyin, D. Kujawski, Generalization of notch analysis and its extension to cyclic loading, *Eng Fract Mech*, 32 (1989) 819-826.
- [45] R. Branco, J.D. Costa, F. Berto, F.V. Antunes, Fatigue life assessment of notched round bars under multiaxial loading based on the total strain energy density approach, *Theor Appl Fract Mec*, 97 (2018) 340-348.
- [46] P. Lazzarin, R. Zambardi, A finite-volume-energy based approach to predict the static and fatigue behavior of components with sharp V-shaped notches, *Int J Fracture*, 112 (2001) 275-298.
- [47] P. Lazzarin, A. Campagnolo, F. Berto, A comparison among some recent energy-and stress-based

- criteria for the fracture assessment of sharp V-notched components under Mode I loading, *Theor Appl Fract Mec*, 71 (2014) 21-30.
- [48] F. Berto, P. Lazzarin, M. Ayatollahi, Brittle fracture of sharp and blunt V-notches in isostatic graphite under torsion loading, *Carbon*, 50 (2012) 1942-1952.
- [49] G. Meneghetti, A. Campagnolo, F. Berto, Averaged strain energy density estimated rapidly from the singular peak stresses by FEM: Cracked bars under mixed-mode (I+ III) loading, *Eng Fract Mech*, 167 (2016) 20-33.
- [50] G. Meneghetti, C. Guzzella, The peak stress method to estimate the mode I notch stress intensity factor in welded joints using three-dimensional finite element models, *Eng Fract Mech*, 115 (2014) 154-171.
- [51] G. Meneghetti, The peak stress method for fatigue strength assessment of tube-to-flange welded joints under torsion loading, *Welding in the World Le Soudage Dans Le Monde*, 57 (2013) 265-275.
- [52] B. Atzori, F. Berto, P. Lazzarin, M. Quaresimin, Multi-axial fatigue behaviour of a severely notched carbon steel, *Int J Fatigue*, 28 (2006) 485-493.
- [53] F. Berto, P. Lazzarin, Fatigue strength of structural components under multi-axial loading in terms of local energy density averaged on a control volume, *Int J Fatigue*, 33 (2011) 1055-1065.
- [54] P. Lazzarin, P. Livieri, F. Berto, M. Zappalorto, Local strain energy density and fatigue strength of welded joints under uniaxial and multiaxial loading, *Eng Fract Mech*, 75 (2008) 1875-1889.
- [55] E. Macha, C. Sonsino, Energy criteria of multiaxial fatigue failure, *Fatigue Fract Eng M*, 22 (1999) 1053-1070.
- [56] F. Berto, P. Lazzarin, J. Yates, Multiaxial fatigue of V-notched steel specimens: a non-conventional application of the local energy method, *Fatigue Fract. Eng. Mater. Struct*, 34 (2011) 921-943.
- [57] F. Berto, A. Campagnolo, P. Lazzarin, Fatigue strength of severely notched specimens made of Ti-6Al-4V under multiaxial loading, *Fatigue Fract Eng M*, 38 (2015) 503-517.
- [58] W. Song, X. Liu, F. Berto, P. Wang, J. Xu, H. Fang, Strain energy density based fatigue cracking assessment of load-carrying cruciform welded joints, *Theor Appl Fract Mec*, 90 (2017) 142-153.
- [59] D. Bellett, D. Taylor, S. Marco, E. Mazzeo, J. Guillois, T. Pircher, The fatigue behaviour of three-dimensional stress concentrations, *Int J Fatigue*, 27 (2005) 207-221.
- [60] P. Lazzarin, C. Sonsino, R. Zambardi, A notch stress intensity approach to assess the multiaxial fatigue strength of welded tube - to - flange joints subjected to combined loadings, *Fatigue Fract Eng M*, 27 (2004) 127-140.
- [61] P. Lazzarin, F. Berto, M. Zappalorto, Rapid calculations of notch stress intensity factors based on averaged strain energy density from coarse meshes: Theoretical bases and applications, *Int J Fatigue*, 32 (2010) 1559-1567.

- [62] D. Taylor, G. Wang, The validation of some methods of notch fatigue analysis, *Fatigue Fract Eng M*, 23 (2000) 387-394.
- [63] L. Susmel, D. Taylor, Fatigue design in the presence of stress concentrations, *The Journal of Strain Analysis for Engineering Design*, 38 (2003) 443-452.
- [64] D. Taylor, P. Bologna, K.B. Knani, Prediction of fatigue failure location on a component using a critical distance method, *Int J Fatigue*, 22 (2000) 735-742.
- [65] Shen Xu, Shun-Peng Zhu, Yong-Zhen Hao, Ding Liao, G. Qian, A new critical plane-energy model for multiaxial fatigue life prediction of turbine disc alloys, *Eng Fail Anal*, 93 (2018) 55-63.
- [66] K. Walat, M. Kurek, P. Ogonowski, T. Łagoda, The multiaxial random fatigue criteria based on strain and energy damage parameters on the critical plane for the low-cycle range, *Int J Fatigue*, 37 (2012) 100-111.
- [67] D. Socie, G. Marquis, *Multiaxial Fatigue*, Society of Automotive Engineers, Inc. Warrendale, Pa, 484 (2000).
- [68] M.W. Brown, K. Miller, A theory for fatigue failure under multiaxial stress-strain conditions, *Proceedings of the Institution of Mechanical Engineers*, 187 (1973) 745-755.
- [69] D. Socie, Multiaxial fatigue damage models, *J. Eng. Mater. Technol.*, 109 (1987) 293-298.
- [70] S.P. Zhu, Z.Y. Yu, J. Correia, A.D. Jesus, F. Berto, Evaluation and comparison of critical plane criteria for multiaxial fatigue analysis of ductile and brittle materials, *Int J Fatigue*, 112 (2018) 279-288.
- [71] L. Susmel, P. Lazzarin, A bi - parametric Wöhler curve for high cycle multiaxial fatigue assessment, *Fatigue Fract Eng M*, 25 (2002) 63-78.
- [72] P. Lazzarin, L. Susmel, A stress - based method to predict lifetime under multiaxial fatigue loadings, *Fatigue Fract Eng M*, 26 (2003) 1171-1187.
- [73] L. Susmel, N. Petrone, Multiaxial fatigue life estimations for 6082-T6 cylindrical specimens under in-phase and out-of-phase biaxial loadings, in: A. Carpinteri, M. de Freitas, A. Spagnoli (Eds.) *European Structural Integrity Society*, Elsevier, 2003, pp. 83-104.
- [74] L. Susmel, Multiaxial fatigue limits and material sensitivity to non - zero mean stresses normal to the critical planes, *Fatigue Fract Eng M*, 31 (2008) 295-309.
- [75] T. Łagoda, E. Macha, A. Dragon, J. Petit, Influence of correlations between stresses on calculated fatigue life of machine elements, *Int J Fatigue*, 18 (1996) 547-555.
- [76] K. Bel Knani, D. Benasciutti, A. Signorini, R. Tovo, Fatigue damage assessment of a car body-in-white using a frequency-domain approach, *International Journal of Materials and Product Technology*, 30 (2007) 172-198.

- [77] D. Benasciutti, R. Tovo, Spectral methods for lifetime prediction under wide-band stationary random processes, *Int J Fatigue*, 27 (2005) 867-877.
- [78] D. Benasciutti, R. Tovo, Cycle distribution and fatigue damage assessment in broad-band non-Gaussian random processes, *Probabilist Eng Mech*, 20 (2005) 115-127.
- [79] L. Susmel, *Multiaxial notch fatigue*, Elsevier, 2009.
- [80] B. Gross, A. Mendelson, Plane elastostatic analysis of V-notched plates, *International Journal of Fracture Mechanics*, 8 (1972) 267-276.
- [81] P. Lazzarin, R. Tovo, A notch intensity factor approach to the stress analysis of welds, *Fatigue Fract Eng M*, 21 (1998) 1089-1103.
- [82] M.L. Dunn, W. Suwito, S. Cunningham, Stress intensities at notch singularities, *Eng Fract Mech*, 57 (1997) 417-430.
- [83] F. Berto, P. Lazzarin, R. Tovo, Multiaxial fatigue strength of severely notched cast iron specimens, *Int J Fatigue*, 67 (2014) 15-27.
- [84] L. Susmel, D. Taylor, A simplified approach to apply the theory of critical distances to notched components under torsional fatigue loading, *Int J Fatigue*, 28 (2006) 417-430.
- [85] Y. Yamashita, Y. Ueda, H. Kuroki, M. Shinozaki, Fatigue life prediction of small notched Ti-6Al-4V specimens using critical distance, *Eng Fract Mech*, 77 (2010) 1439-1453.
- [86] R. Negru, D.A. Şerban, L. Marşavina, A. Magda, Lifetime prediction in medium-cycle fatigue regime of notched specimens, *Theor Appl Fract Mec*, 84 (2016) 140-148.
- [87] P. Livieri, E. Salvati, R. Tovo, A non-linear model for the fatigue assessment of notched components under fatigue loadings, *Int J Fatigue*, 82 (2016) 624-633.
- [88] M. Yu, D. DuQuesnay, T. Topper, Notched fatigue behaviour of two cold rolled steels, *Fatigue Fract Eng M*, 14 (1991) 89-101.
- [89] D.L. DuQuesnay, T.H. Topper, M. Yu, A.M. Bertetto, The effect of notch radius on the fatigue notch factor and the propagation of short cracks, in: *EGF1*, 1986.
- [90] G. Meneghetti, M. Ricotta, B. Atzori, A synthesis of the push-pull fatigue behaviour of plain and notched stainless steel specimens by using the specific heat loss, *Fatigue Fract Eng M*, 36 (2013) 1306-1322.
- [91] K. Tokaji, Notch fatigue behaviour in a Sb-modified permanent-mold cast A356-T6 aluminium alloy, *Materials Science and Engineering: A*, 396 (2005) 333-340.
- [92] J. Denk, J. Dallmeier, O. Huber, H. Saage, The fatigue life of notched magnesium sheet metals with emphasis on the effect of bands of twinned grains, *Int J Fatigue*, 98 (2017) 212-222.

- [93] G. Gasiak, R. Pawliczek, The mean loading effect under cyclic bending and torsion of 18G2A steel, 6th Int, in: Conf. on Biaxial/Multiaxial Fatigue and Fracture, 2001, pp. 213-222.
- [94] F. Berto, P. Lazzarin, J. Yates, Multiaxial fatigue of V - notched steel specimens: a non - conventional application of the local energy method, *Fatigue Fract Eng M*, 34 (2011) 921-943.
- [95] P. Kurath, S. Downing, D. Galliard, Summary of non-hardened notched shaft round robin program, Society of Automotive Engineers, Inc., *Multiaxial Fatigue: Analysis and Experiments*, (1989) 13-31.
- [96] N.R. Gates, A. Fatemi, On the consideration of normal and shear stress interaction in multiaxial fatigue damage analysis, *Int J Fatigue*, 100 (2017) 322-336.
- [97] M. Chaudonneret, A simple and efficient multiaxial fatigue damage model for engineering applications of macro-crack initiation, *J. Eng. Mater. Technol.*, 115 (1993) 373-379.
- [98] D. Kardas, K. Kluger, T. Łagoda, P. Ogonowski, Fatigue life of AlCu4Mg1 aluminium alloy under constant amplitude bending with torsion, in: *Proced. of the Seventh International Conference on Biaxial/Multiaxial Fatigue and Fracture*, 2004, pp. 197-202.
- [99] Y.Y. Wang, W.X. Yao, A multiaxial fatigue criterion for various metallic materials under proportional and nonproportional loading, *Int J Fatigue*, 28 (2006) 401-408.
- [100] D. Socie, P. Kurath, J. Koch, A multiaxial fatigue damage parameter, in: *ICBMFF2*, 1985.
- [101] G. Qilafku, N. Kadi, J. Dobranski, Z. Azari, M. Gjonaj, G. Pluvinage, Fatigue of specimens subjected to combined loading. Role of hydrostatic pressure, *Int J Fatigue*, 23 (2001) 689-701.
- [102] S.B. Lee, A criterion for fully reversed out-of-phase torsion and bending, in: *Multiaxial Fatigue*, ASTM International, 1985.
- [103] K.S. Kim, X. Chen, C. Han, H.W. Lee, Estimation methods for fatigue properties of steels under axial and torsional loading, *Int J Fatigue*, 24 (2002) 783-793.
- [104] A. Fatemi, R. Molaei, S. Sharifimehr, N. Phan, N. Shamsaei, Multiaxial fatigue behavior of wrought and additive manufactured Ti-6Al-4V including surface finish effect, *Int J Fatigue*, 100 (2017) 347-366.

List of captions

Table1. Synthesis of the experimental results of notched specimens under uniaxial loading calculated by TCD.

Table2. Synthesis of the experimental results of notched specimens under uniaxial loading calculated by SED.

Table3. Parameters of the fatigue curves related to the plain specimens.

Table4. Synthesis of the experimental results of plain specimens under multiaxial loading calculated by SED.

Table5. Values of the fatigue constants used to apply the MWCM in conjunction with the PM to the considered materials.

Table6. Synthesis of the experimental results of notched specimens under multiaxial loading calculated by SED.

Figure1. Calibration method of the critical distance using plain and notched fatigue curve.

Figure2. Flow-chart summarizing the procedure used to estimate fatigue lifetime according to the TCD.

Figure3. Critical volume (area) for sharp V-notch (a), crack (b) and blunt V-notch (c) under mode I loading. Distance $r_0 = \rho \times (\pi - 2\alpha) / (2\pi - 2\alpha)$.

Figure4. Calibration method of the control radius of the critical volume by using FEA.

Figure5. Flow-chart summarizing the procedure used to estimate fatigue lifetime according to the SED.

Figure6. PM and LM accuracy in predicting fatigue lifetime of notched specimens.

Figure7. SED accuracy in predicting fatigue lifetime of notched specimens.

Figure8. Probability density function of errors of predicting fatigue lifetime according to TCD and SED.

Figure9. Flow-chart summarizing the in-field use of the MWCM method.

Figure10. In-field use of the MWCM in terms of the PM to estimate fatigue lifetime of the notched components subjected to fatigue loading.

Figure11. Polar coordination system for V-notches, with z normal to the plane; the stress component σ_θ is evaluated along the notch bisector line ($\theta=0$) for mode I NSIF; the shear stress component $\tau_{z\theta}$ is oriented as σ_θ .

Figure12. MWCM accuracy in predicting fatigue lifetime of plain specimens under multiaxial loading.

Figure13. SED accuracy in predicting fatigue lifetime of plain specimens under multiaxial loading.

Figure14. Probability density function of errors of predicting fatigue lifetime of plain specimens under multiaxial loading according to MWCM and SED.

Figure15. MWCM accuracy in predicting fatigue lifetime of notched specimens under multiaxial loading.

Figure16. SED accuracy in predicting fatigue lifetime of notched specimens under multiaxial loading.

Figure17. Probability density function of errors of predicting fatigue lifetime of notched specimens under multiaxial loading according to MWCM and SED.

Table 1 Synthesis of the experimental results of notched specimens under uniaxial loading calculated by TCD.

Material	R	L versus N_f relationship	Specimen geometry	Load type
Ti6Al4V[85]	0	PM: $L(N_f)=0.058 \times N_f^{0.08709}$ LM: $L(N_f)=0.047 \times N_f^{0.0922}$	V-notched cylindrical bars	Tension
2024-T3[86]	0.5	PM: $L(N_f)=5.72 \times N_f^{-0.28605}$ LM: $L(N_f)=7.72 \times N_f^{-0.34163}$	U and V-notched plates	Tension- compression
FeP04[87]	0	PM: $L(N_f)=70.76 \times N_f^{-0.32783}$ LM: $L(N_f)=45.50 \times N_f^{-0.30299}$	U and V-notched plates	Tension
SAE 1010CR22[88]	-1	PM: $L(N_f)=2.58 \times N_f^{-0.18345}$ LM: $L(N_f)=13.82 \times N_f^{-0.32164}$	Plates with a central circular hole	Tension- compression
SAE 1010HR[88]	-1	PM: $L(N_f)=7.68 \times N_f^{-0.17794}$ LM: $L(N_f)=20.42 \times N_f^{-0.26631}$	Plates with a central circular hole	Tension- compression
SAE 1045[89]	-1	PM: $L(N_f)=100.28 \times N_f^{-0.49868}$ LM: $L(N_f)=176.02 \times N_f^{-0.56547}$	Plates with a central circular hole	Tension- compression
2024-T351[89]	-1	PM: $L(N_f)=0.26 \times N_f^{-0.10104}$ LM: $L(N_f)=0.18 \times N_f^{-0.10095}$	Plates with a central circular hole	Tension- compression
AISI 304L[90]	-1	PM: $L(N_f)=128.64 \times N_f^{-0.35662}$ LM: $L(N_f)=70.53 \times N_f^{-0.3258}$	Central circular hole, U and V- notched plates	Tension- compression
AISI 416[53]	-1	PM: $L(N_f)=642.94 \times N_f^{-0.624317}$ LM: $L(N_f)=179.25 \times N_f^{-0.514785}$	V-notched cylindrical bars	Tension- compression
A356-T6[91]	-1	PM: $L(N_f)=1.78 \times N_f^{-0.07359}$ LM: $L(N_f)=1.93 \times N_f^{-0.08838}$	U and V-notched cylindrical bars	Tension- compression
AM50 Magnesium[92]	-1	PM: $L(N_f)=19.36 \times N_f^{-0.33804}$ LM: $L(N_f)=56.62 \times N_f^{-0.47577}$	Plates with a central hole	Tension- compression

Table 2 Synthesis of the experimental results of notched specimens under uniaxial loading calculated by SED.

Material	W versus N_f relationship	c_w	T_σ	T_w	$R_0(\text{mm})$
Ti6Al4V[85]	SED: $W(N_f)=201.79 \times N_f^{-0.23175}$	1	Plain:1.29 Notch:1.12	1.24	0.0158
2024-T3[86]	SED: $W(N_f)=149.94 \times N_f^{-0.46051}$	3	Plain:1 Notch:1.63	3.2	0.03
FeP04[87]	SED: $W(N_f)=11.89 \times N_f^{-0.3794}$	1	Plain:1.08 Notch:1.15	1.33	0.44
SAE 1010CR22[88]	SED: $W(N_f)=2.44 \times N_f^{-0.23423}$	0.5	Plain:1.10 Notch:1.26	1.6	0.16
SAE 1010HR[88]	SED: $W(N_f)=2.90 \times N_f^{-0.31333}$	0.5	Plain:1.34 Notch:1.12	1.25	0.36
SAE 1045[89]	SED: $W(N_f)=67.55 \times N_f^{-0.34875}$	0.5	Plain:1.24 Notch:1.1	1.24	0.139
2024-T351[89]	SED: $W(N_f)=39.92 \times N_f^{-0.33783}$	0.5	Plain:1.78 Notch:1.21	1.48	0.21
AISI 304L[90]	SED: $W(N_f)=5.80 \times N_f^{-0.3485}$	0.5	Plain:1.03 Notch:1.17	1.36	3.1
AISI 416[53]	SED: $W(N_f)=300.67 \times N_f^{-0.49467}$	0.5	Plain:1.12 Notch:1.47	2.16	0.13
A356-T6[91]	SED: $W(N_f)=7.12 \times N_f^{-0.3446}$	0.5	Plain:1.46 Notch:1.82	3.3	0.35
AM50 Magnesium[92]	SED: $W(N_f)=0.053 \times N_f^{-0.45299}$	0.5	Plain:1.22 Notch:1.54	2.3	0.09

Table 3 Parameters of the fatigue curves related to the plain specimens.

Material	σ_A	τ_A	σ_u	m	Load type	N_A (Cycles)
18G2A[93]	282.6	186.5	535	1	Bending-torsion	2×10^6
39NiCrMo3[94]	346.9	285.3	995	1	Tension-torsion	1×10^6
SAE 1045[95]	195.8	115.8	621	1	Bending-torsion	2×10^6
2024-T3[96]	137.1	131.7	495	1	Tension-torsion	2×10^6
6082-T6[73]	133	76.8	343	1	Bending-torsion	2×10^6
Al 1070[97]	77.9	45.6	130	1	Tension-torsion	2×10^6
AlCu4Mg1[98]	164.6	97.3	545	1	Bending-torsion	2×10^6
Al-LY12CZ[99]	149.4	110.3	459	1	Tension-torsion	2×10^6
Inconel 718[100]	696.4	338.1	1850	1	Tension-torsion	2×10^6
Low-carbon steel[101]	225	145	500	1	Tension-torsion	1×10^6
SM45C[102]	258.6	209.4	731	1	Bending-torsion	2×10^6
S45C[103]	204.7	147.3	798	1	Tension-torsion	1×10^6
Ti6Al4V-as built[104]	107.4	146.4	1052	1	Tension-torsion	1×10^6
Ti6Al4V-wrough[104]	618.7	350	1045	1	Tension-torsion	1×10^6
Ti6Al4V-machined[104]	82.3	177	1052	1	Tension-torsion	1×10^6
Z12CNDV12-2[97]	413.3	296.3	880	1	Tension-torsion	2×10^6

Table 4 Synthesis of the experimental results of plain specimens under multiaxial loading calculated by SED.

Material	W versus N_f relationship	c_w	$T_\sigma(10\%-90\%)$	$T_w(10\%-90\%)$
18G2A[93]	$W(N_f)=6.1 \times N_f^{-0.19431}$	0.5($R=-1$), 0.6($R=-0.5$), 1($R=0$)	1.3	4.2
39NiCrMo3[94]	$W(N_f)=18.56 \times N_f^{-0.22195}$	0.5	1.26	1.58
SAE 1045[95]	$W(N_f)=3.27 \times N_f^{-0.16616}$	0.5	8.01	1.79
2024-T3[96]	$W(N_f)=22.32 \times N_f^{-0.28854}$	0.5	1.34	2.57
6082-T6[73]	$W(N_f)=6.02 \times N_f^{-0.20016}$	0.5	1.98	1.79
Al 1070[97]	$W(N_f)=0.29 \times N_f^{-0.06938}$	0.5	1.41	5.16
AlCu4Mg1[98]	$W(N_f)=29.04 \times N_f^{-0.29571}$	0.5	6.89	1.71
Al-LY12CZ[99]	$W(N_f)=8.59 \times N_f^{-0.19874}$	0.5	1.89	2.42
Inconel 718[100]	$W(N_f)=44.30 \times N_f^{-0.27634}$	0.5	1.57	2.31
Low-carbon steel[101]	$W(N_f)=2.42 \times N_f^{-0.13289}$	0.5	1.21	1.46
SM45C[102]	$W(N_f)=5.01 \times N_f^{-0.16434}$	0.5	1.58	1.23
S45C[103]	$W(N_f)=9.93 \times N_f^{-0.28757}$	0.5	2.13	4.56
Ti6Al4V-as built[104]	$W(N_f)=409.29 \times N_f^{-0.5784}$	0.5	3.44	5.04
Ti6Al4V-wrough[104]	$W(N_f)=10.95 \times N_f^{-0.06631}$	0.5	4.07	12.3
Ti6Al4V-machined[104]	$W(N_f)=14.41 \times N_f^{-0.20008}$	0.5	2.56	6.56
Z12CNDV12-2[97]	$W(N_f)=24.09 \times N_f^{-0.26698}$	0.5	1.83	2.38

Table 5 Values of the fatigue constants used to apply the MWCM in conjunction with the PM to the considered materials.

Material	B	A (mm/cycles ^B)	a	b	α (MPa)	β (MPa)	m	ρ_{lim}	N_A (Cycles)
Ti6Al4V[57]	-0.1019	0.32785	-12.88	22.13	-144.22	400.6	1	1.389	1×10^6
C40 steel[52]	-0.345	48.7	-1.2	17.5	-63.3	194.3	1	1.534	2×10^6
39NiCrMo3[56]	-0.1065	1.5611	-2.31	9.52	-111.89	285.3	1	1.275	1×10^6
En3B[30]	-0.565	118.9	1	18.7	-95.3	268.3	0.22	1.407	1×10^6
AISI416[53]	-0.6243	642.942	6.3	21.2	-62.7	236.9	1	1.889	2×10^6

Table 6 Synthesis of the experimental results of notched specimens under multiaxial loading calculated by SED.

Material	W versus N_f relationship	Specimen geometry	c_w	T_σ (10%-90%)	T_w (10%-90%)	R_1 or R_3 (mm)
Ti6Al4V[57]	$W(N_f)=60.12 \times N_f^{0.21978}$	V-notched cylindrical bars	0.5($R=-1$), 1($R=0$), 3($R=0.5$)	1.322	2.2	0.051,0.8 37
C40 steel[52]	$W(N_f)=61.94 \times N_f^{0.26601}$	V-notched cylindrical bars, shaft	0.5($R=-1$), 1($R=0$)	1.81	2.75	Point criterion
39NiCrMo3[56]	$W(N_f)=22.93 \times N_f^{0.24755}$	V-notched cylindrical bars	0.5($R=-1$), 1($R=0$)	1.53	2.24	0.327,1.4 26
En3B[30]	$W(N_f)=11.62 \times N_f^{0.33444}$	V-notched cylindrical bars	0.5($R=-1$), 1($R=0$)	1.872	3.01	0.33,0.93
En3B[30]	$W(N_f)=4.99 \times N_f^{0.09926}$	V-notched cylindrical bars	0.5($R=-1$), 1($R=0$)	1.998	4.22	Point criterion
AISI416[53]	$W(N_f)=7.33 \times N_f^{0.21619}$	V-notched cylindrical bars	0.5($R=-1$), 1($R=0$)	1.66	2.7	0.13,0.78

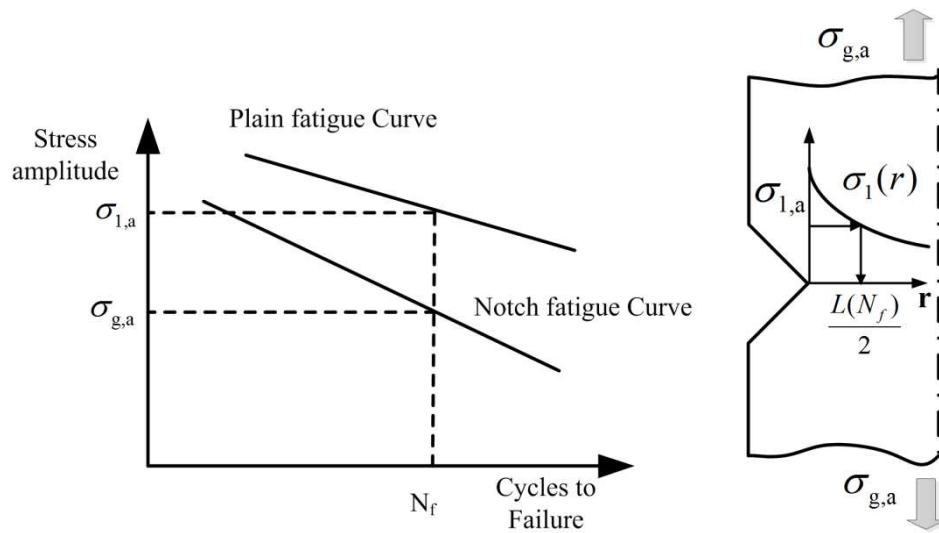


Figure 1 Calibration method of the critical distance using plain and notched fatigue curve.

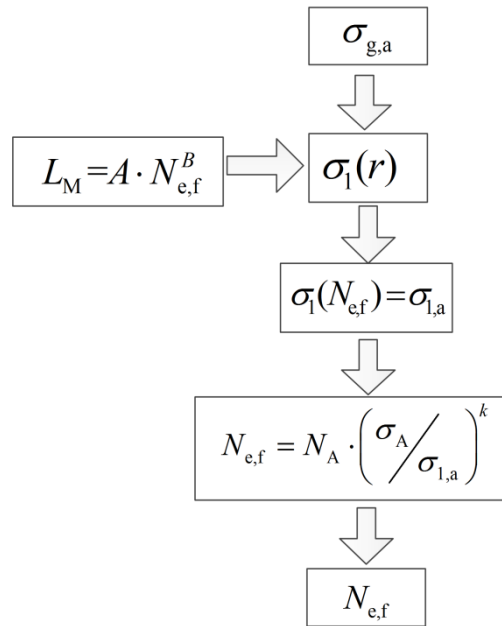


Figure 2 Flow-chart summarizing the procedure used to estimate fatigue lifetime according to the TCD.

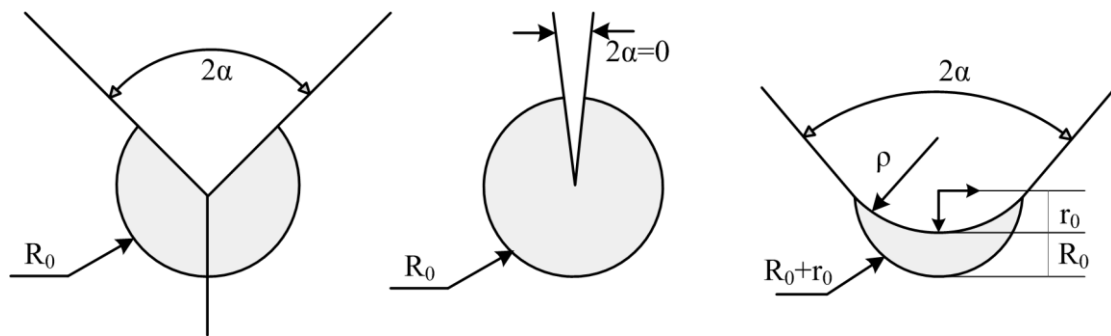


Figure 3 Critical volume (area) for sharp V-notch (a), crack (b) and blunt V-notch (c) under mode I loading. Distance $r_0 = \rho \times (\pi - 2\alpha) / (2\pi - 2\alpha)$.

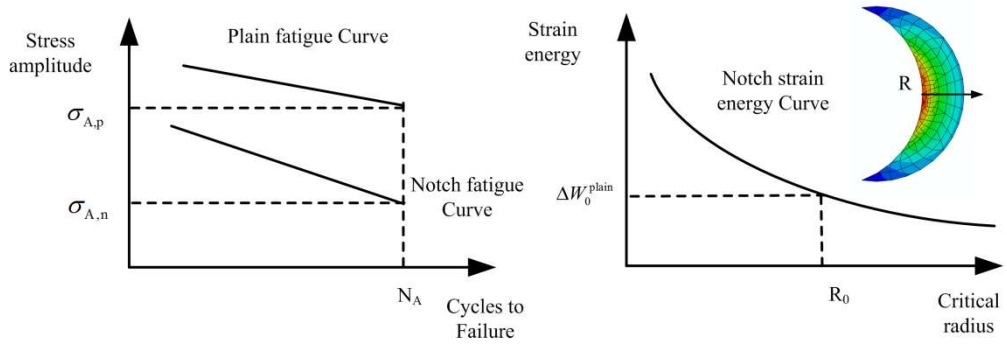


Figure 4 Calibration method of the control radius of the critical volume by using FEA.

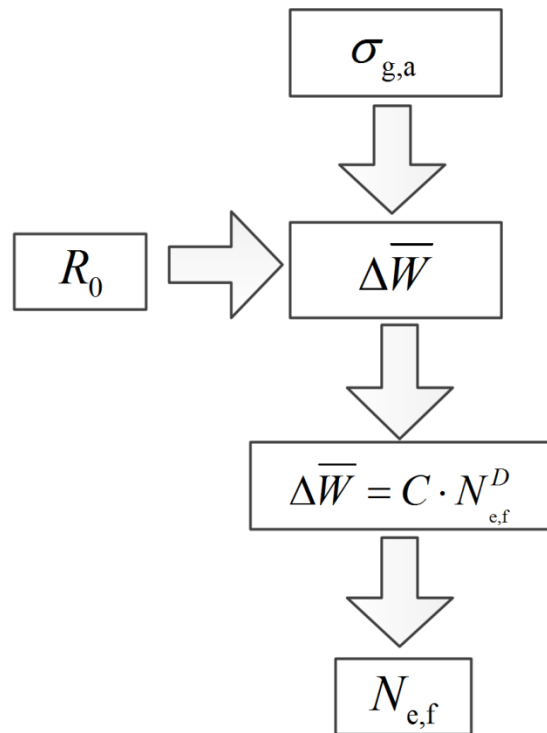
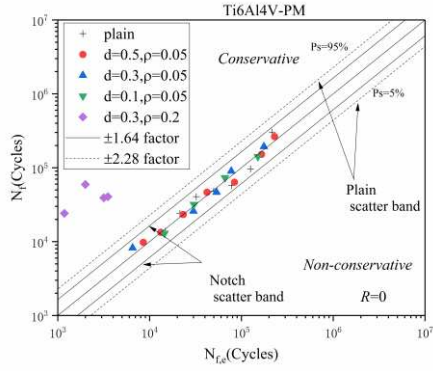
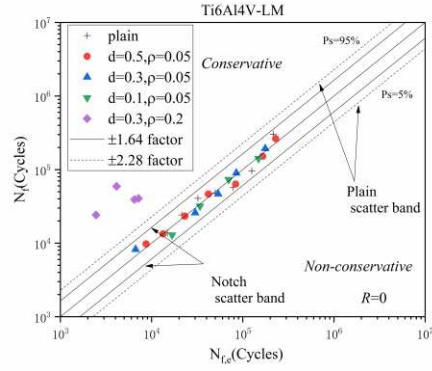


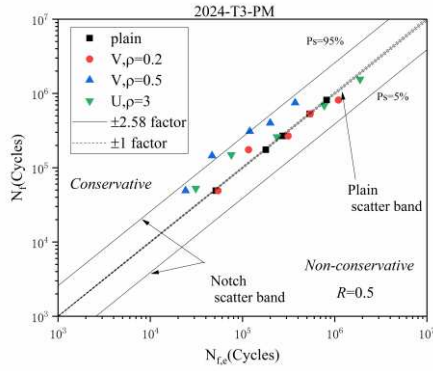
Figure 5 Flow-chart summarizing the procedure used to estimate fatigue lifetime according to the SED.



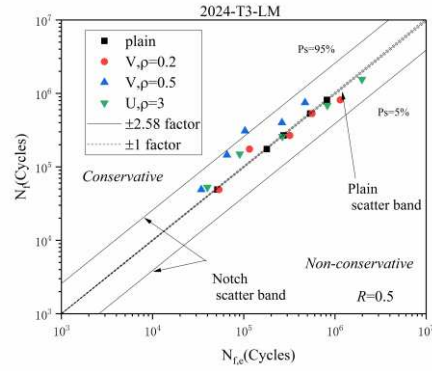
(a)



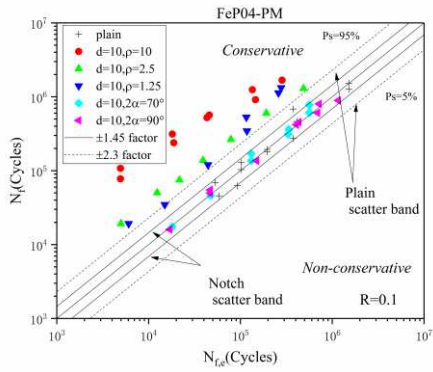
(b)



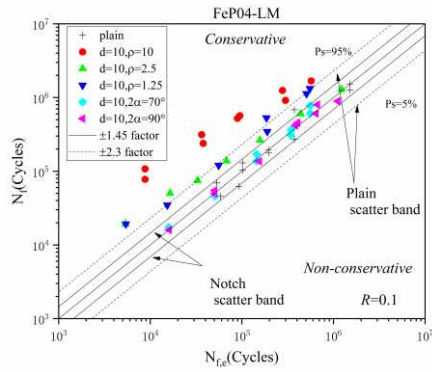
(c)



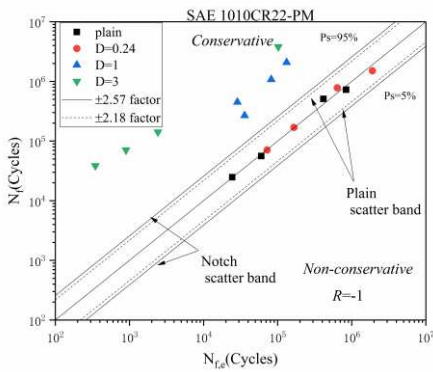
(d)



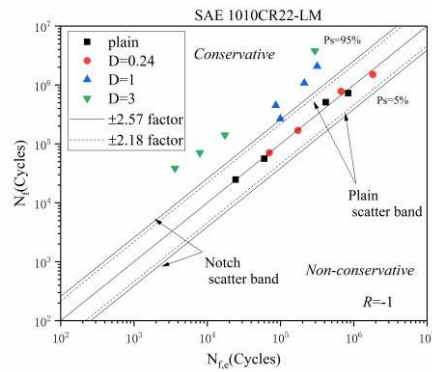
(e)



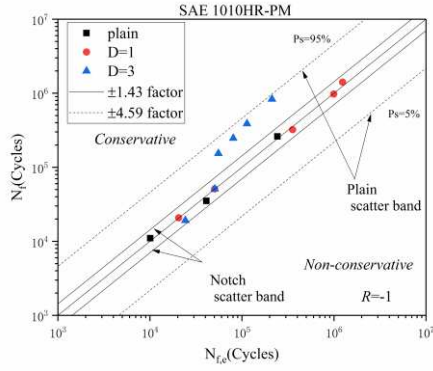
(f)



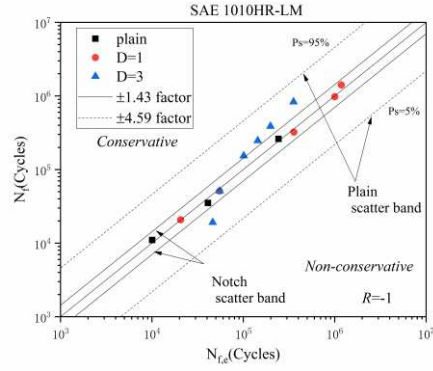
(g)



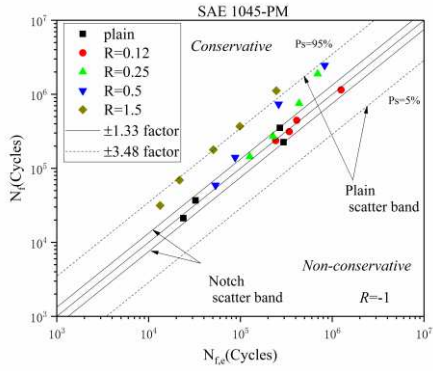
(h)



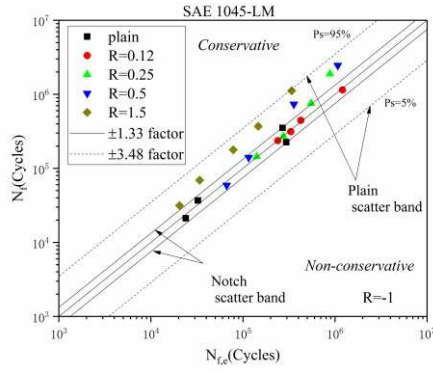
(i)



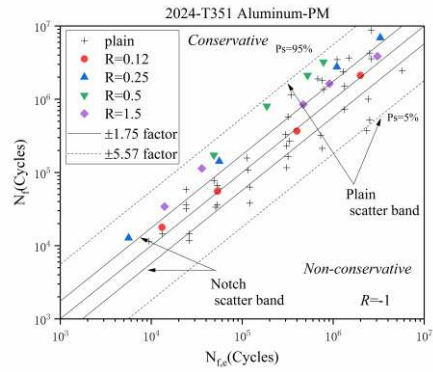
(j)



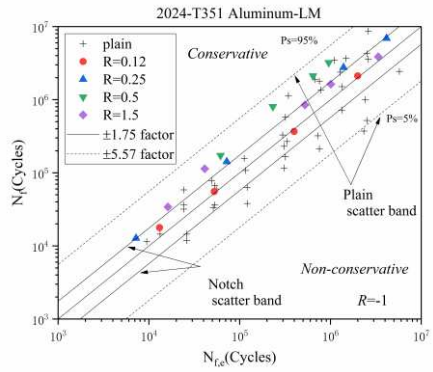
(k)



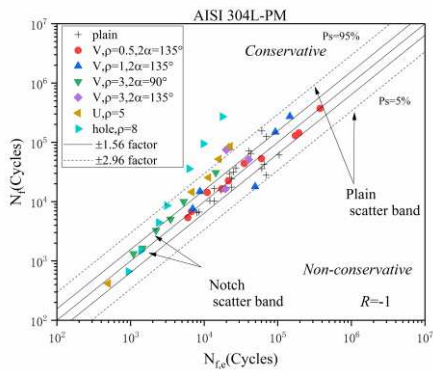
(l)



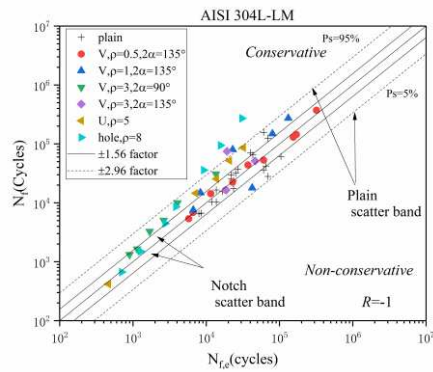
(m)



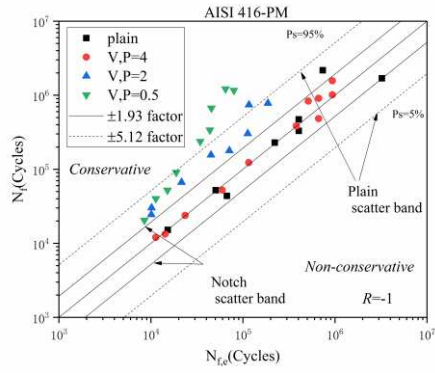
(n)



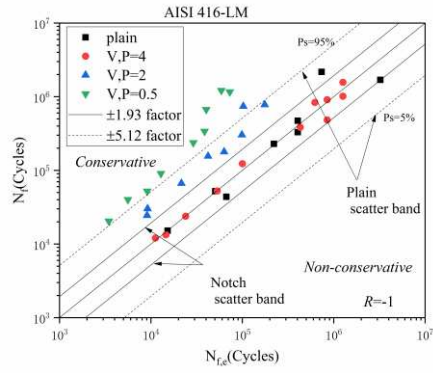
(o)



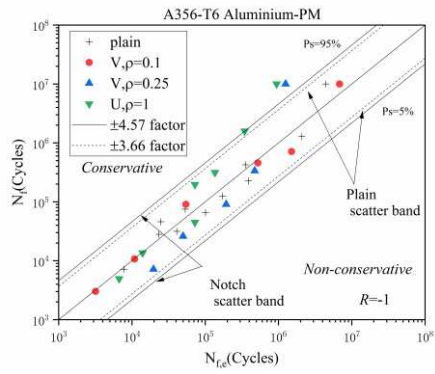
(p)



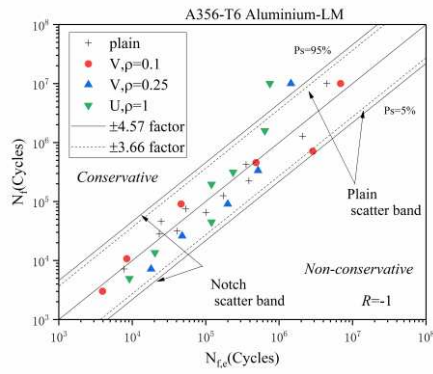
(q)



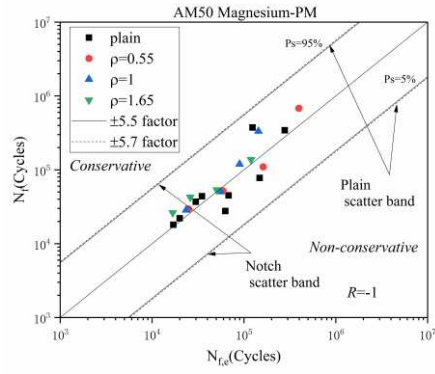
(r)



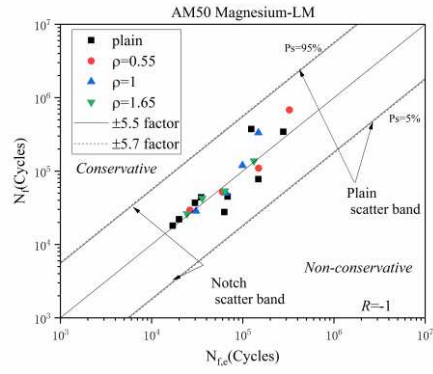
(s)



(t)

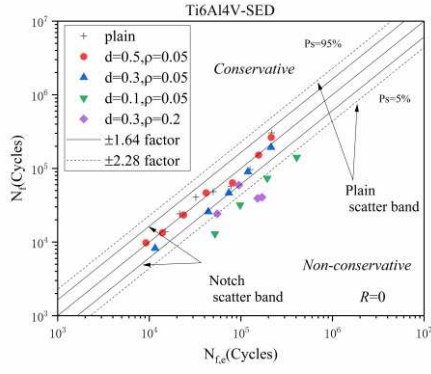


(u)

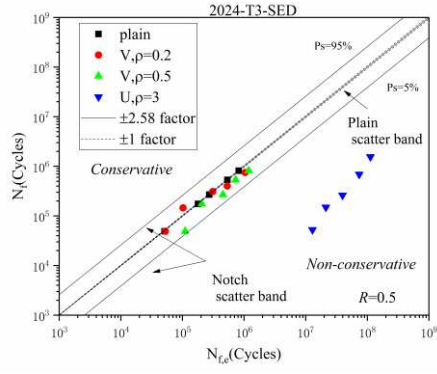


(v)

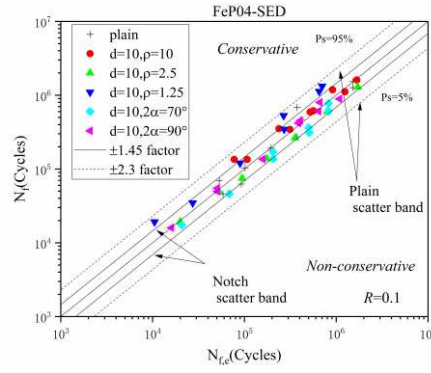
Figure 6 PM and LM accuracy in predicting fatigue lifetime of notched specimens.



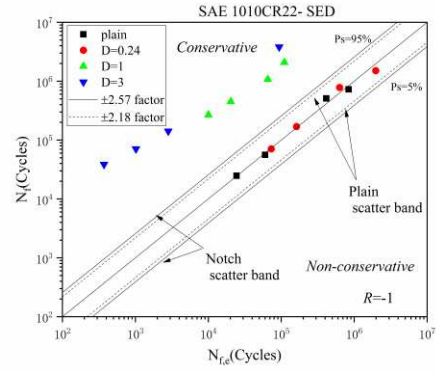
(a)



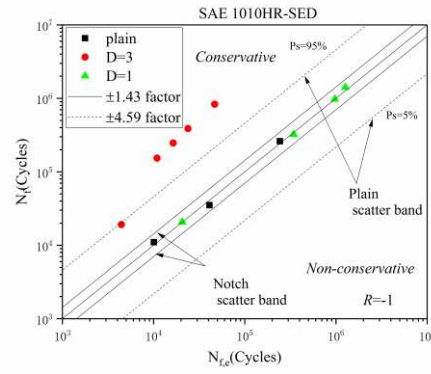
(b)



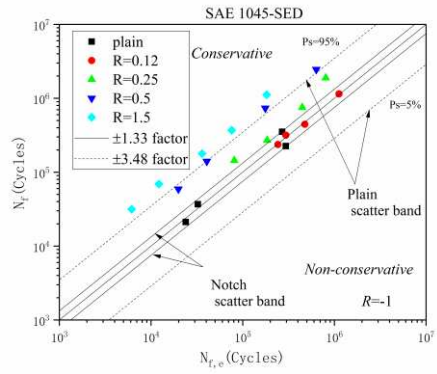
(c)



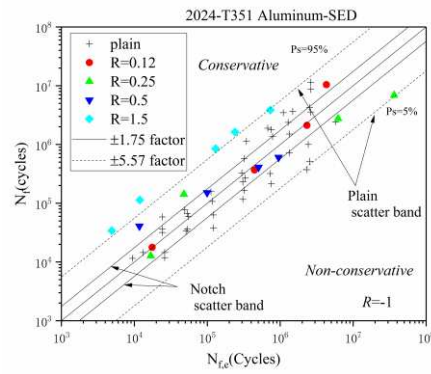
(d)



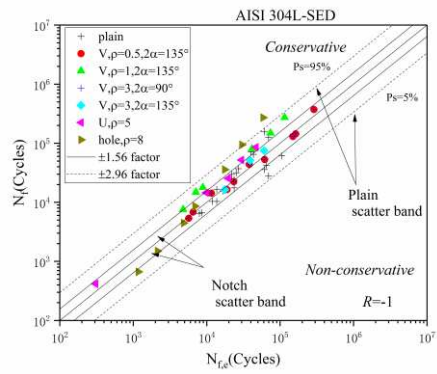
(e)



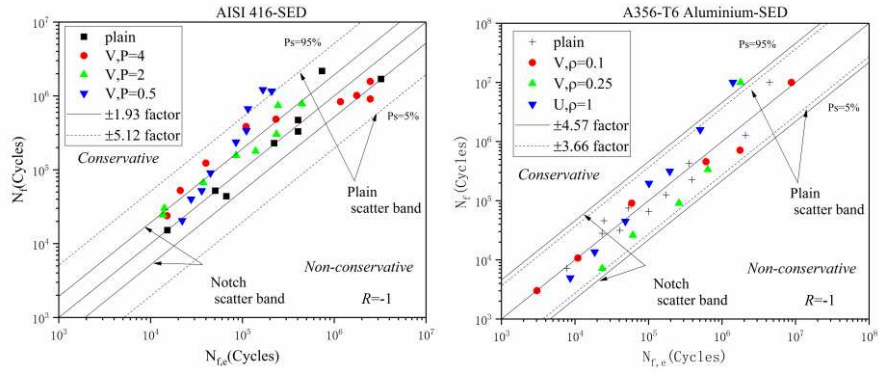
(f)



(g)

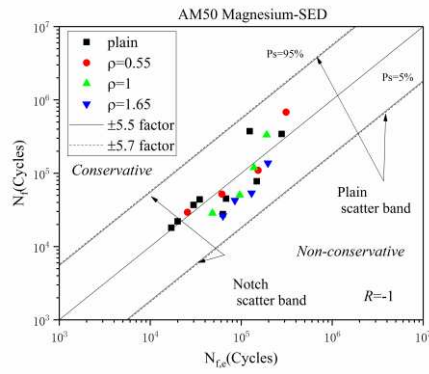


(h)



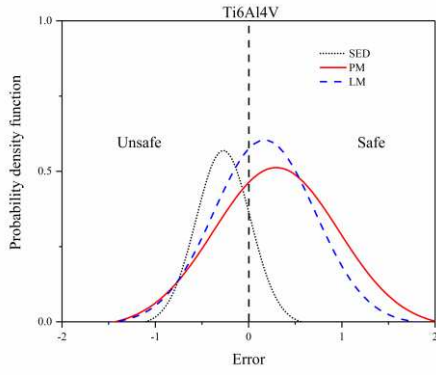
(i)

(j)

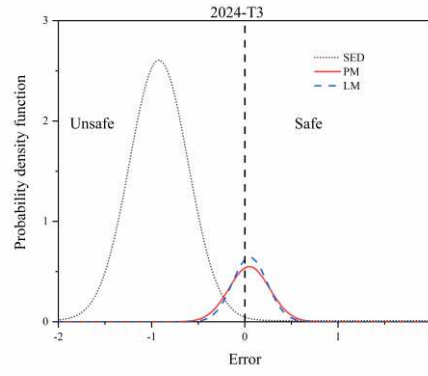


(k)

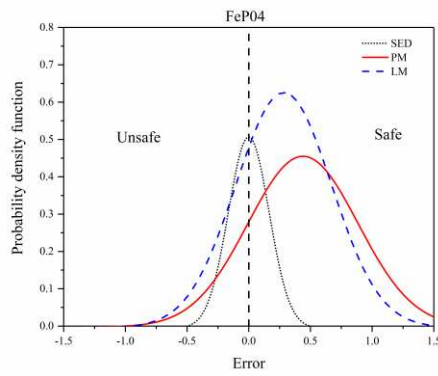
Figure 7 SED accuracy in predicting fatigue lifetime of notched specimens.



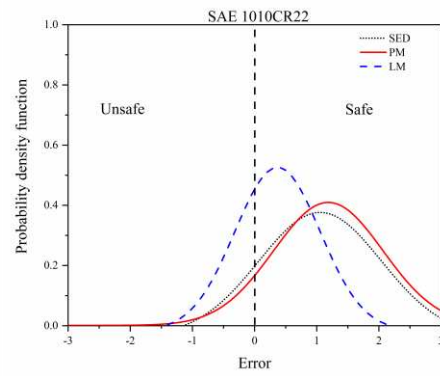
(a)



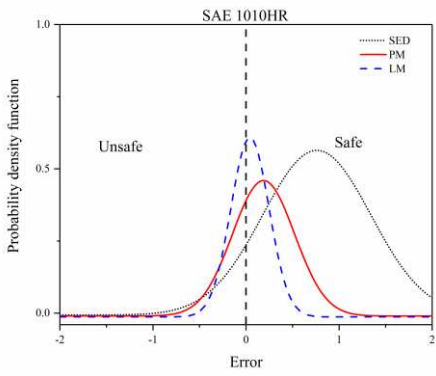
(b)



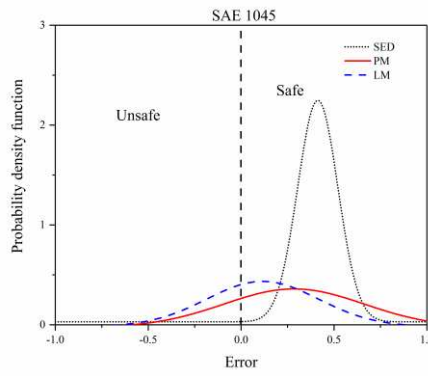
(c)



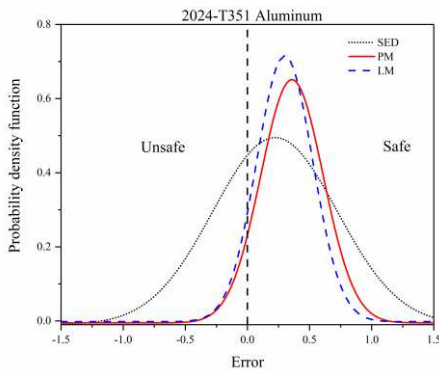
(d)



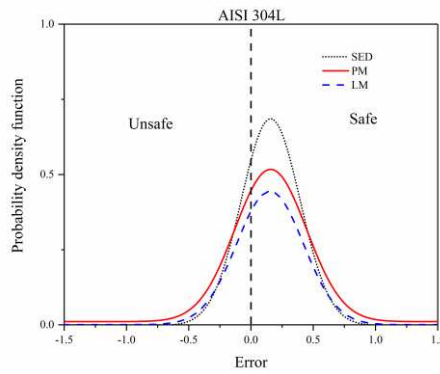
(e)



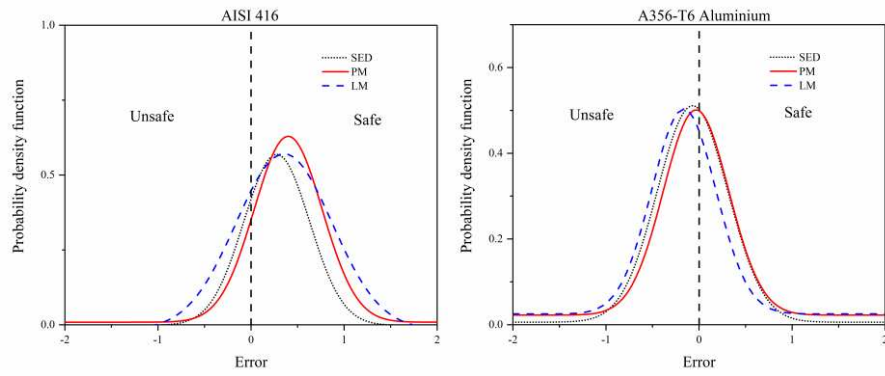
(f)



(g)

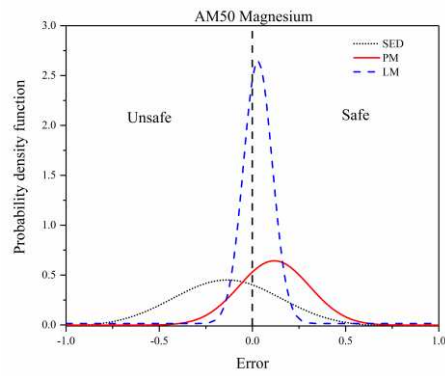


(h)



(i)

(j)



(k)

Figure 8 Probability density function of errors of predicting fatigue lifetime according to TCD and SED.

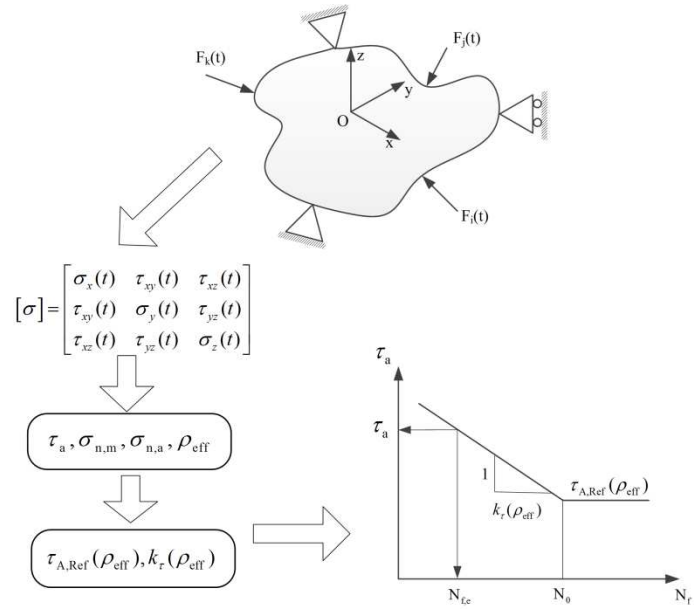


Figure 9 Flow-chart summarizing the in-filed use of the MWCM method.

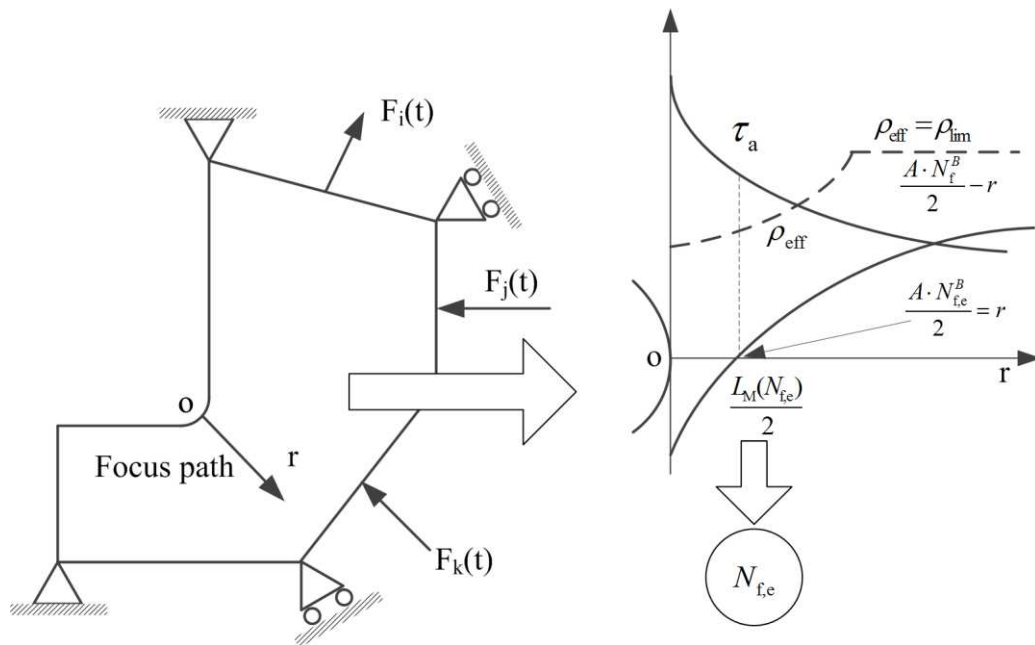


Figure 10 In-field use of the MWCM in terms of the PM to estimate fatigue lifetime of the notched components subjected to fatigue loading.

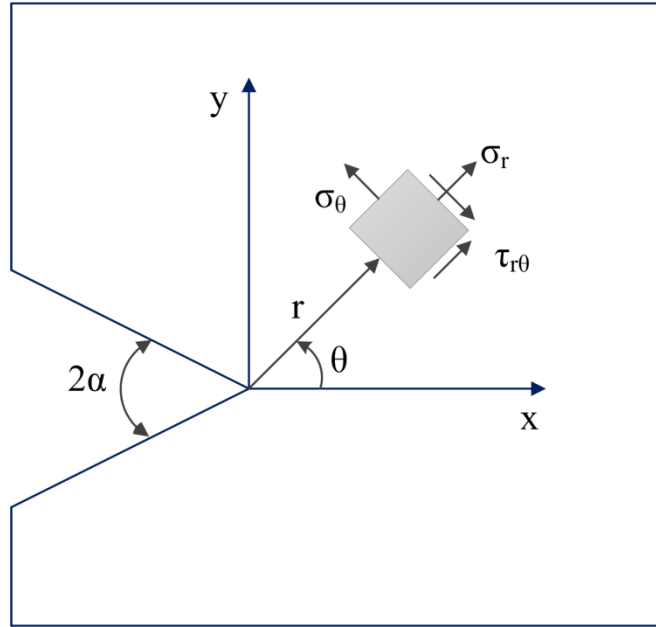
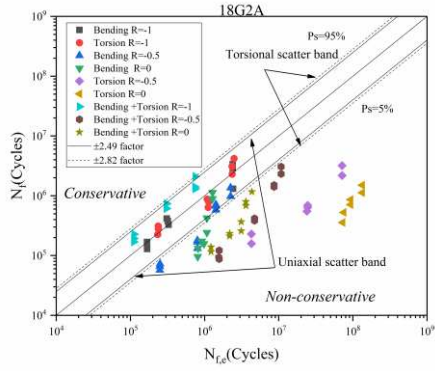
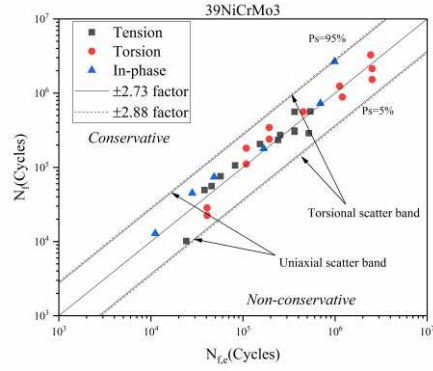


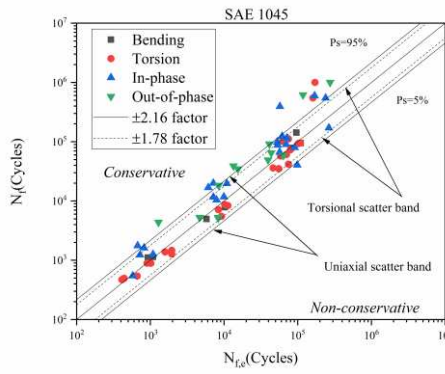
Figure 11 Polar coordination system for V-notches, with z normal to the plane; the stress component σ_θ is evaluated along the notch bisector line ($\theta=0$) for mode I NSIF; the shear stress component $\tau_{z\theta}$ is oriented as σ_θ .



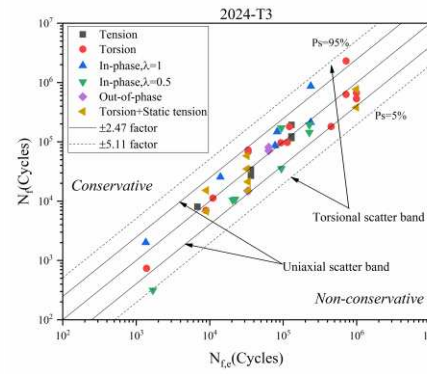
(a)



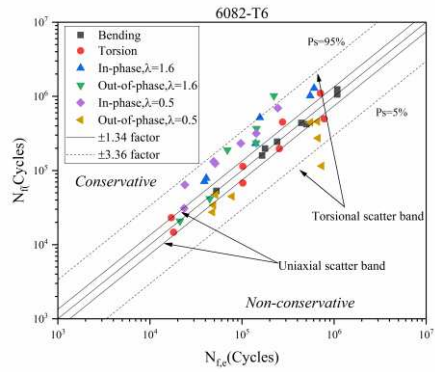
(b)



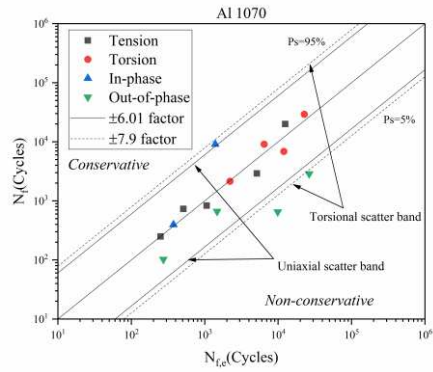
(c)



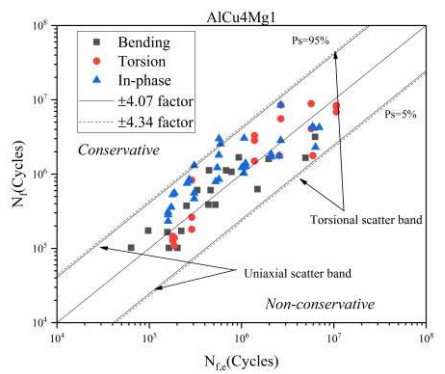
(d)



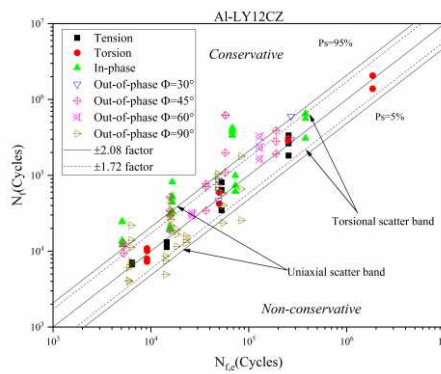
(e)



(f)



(g)



(h)

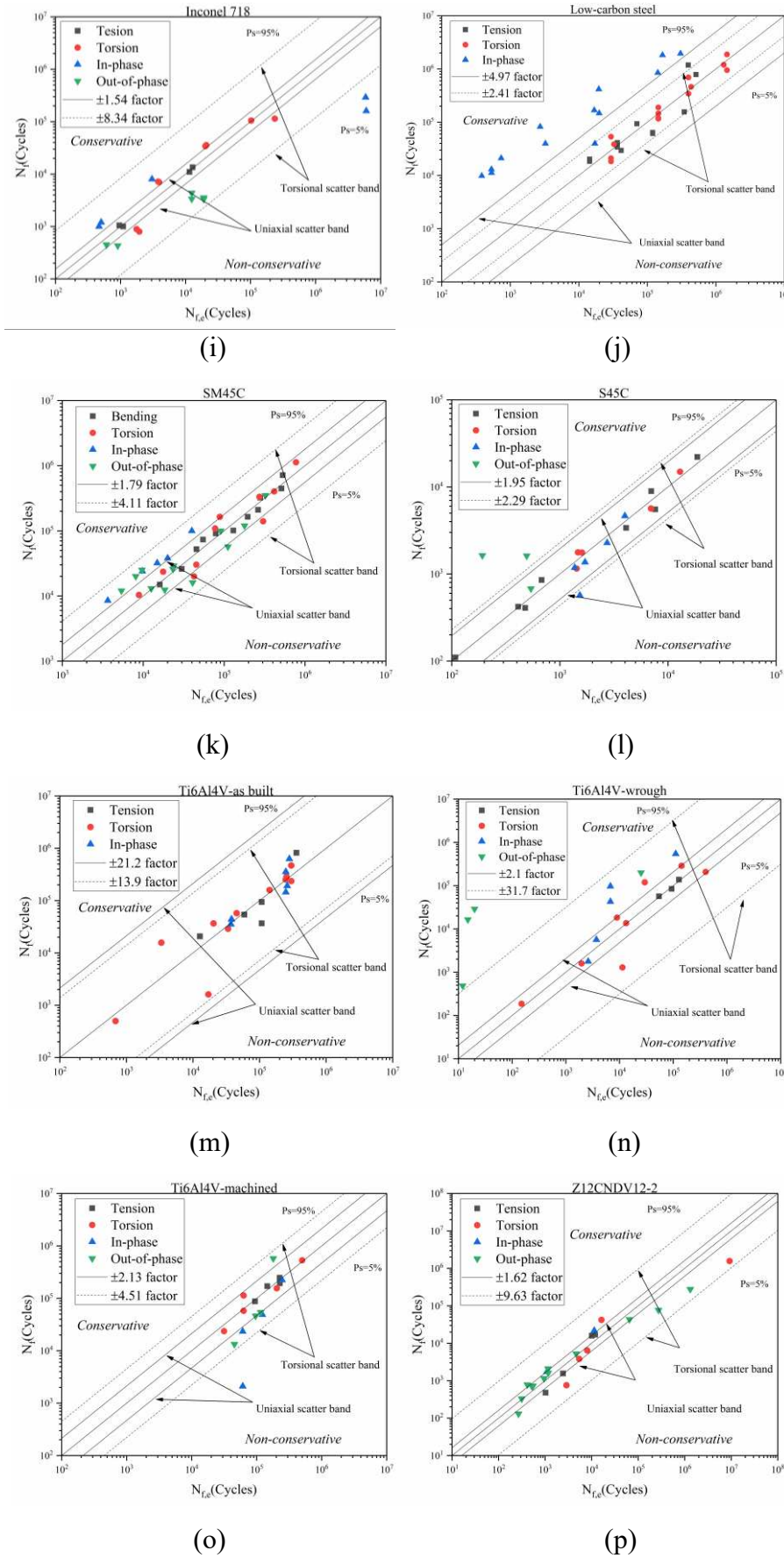
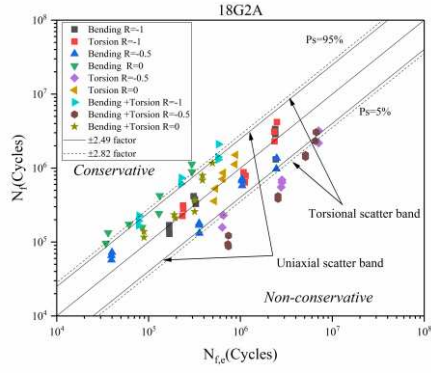
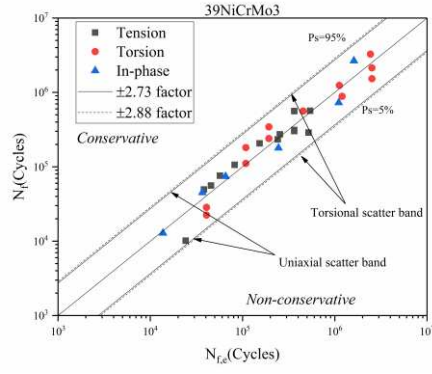


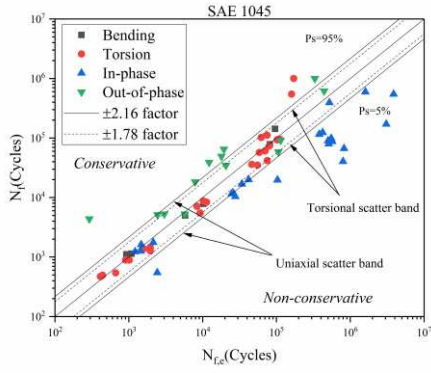
Figure 12 MWCM accuracy in predicting fatigue lifetime of plain specimens under multiaxial loading.



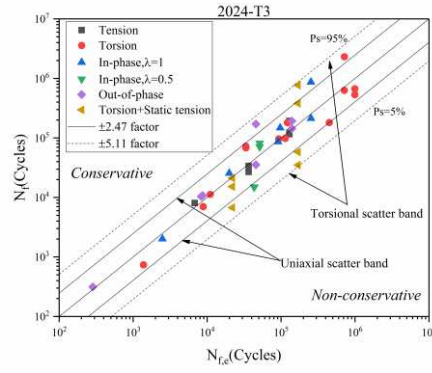
(a)



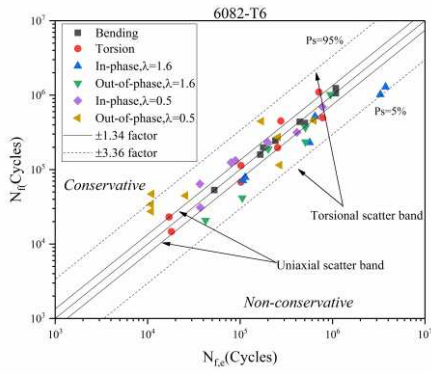
(b)



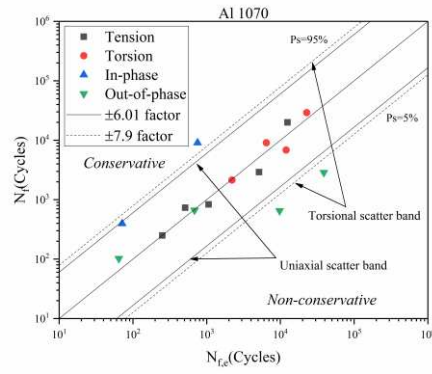
(c)



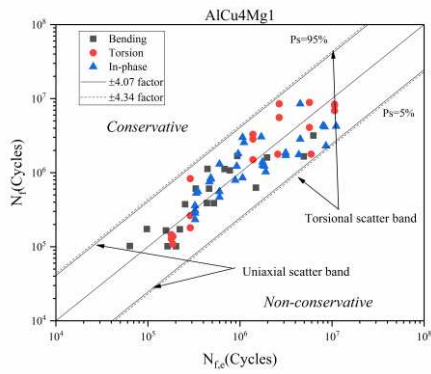
(d)



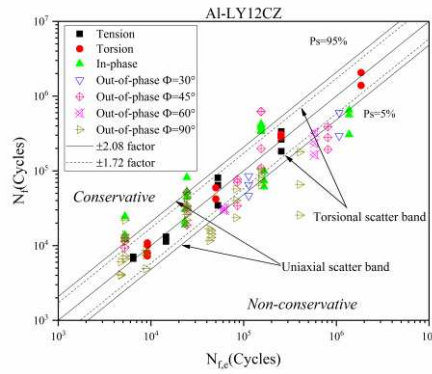
(e)



(f)



(g)



(h)

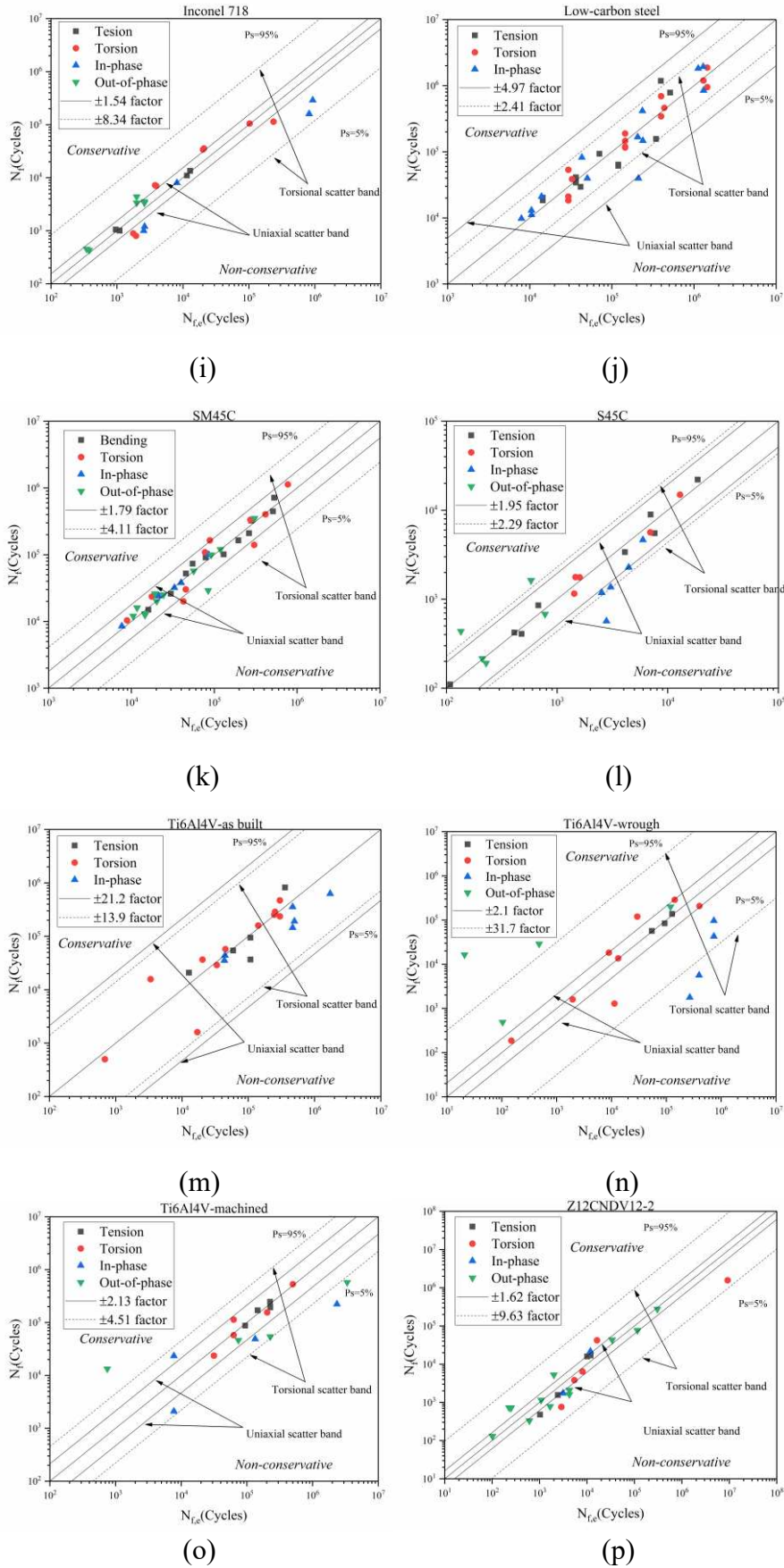
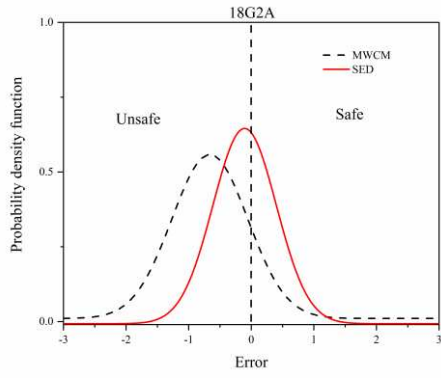
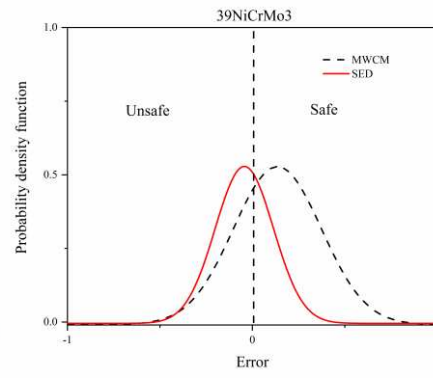


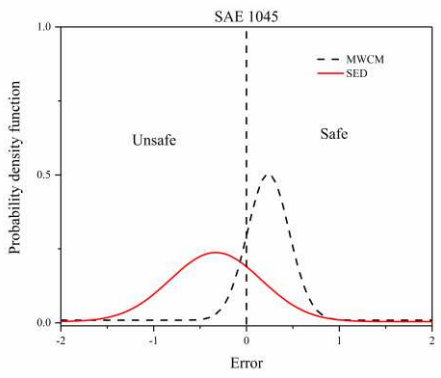
Figure 13 SED accuracy in predicting fatigue lifetime of plain specimens under multiaxial loading.



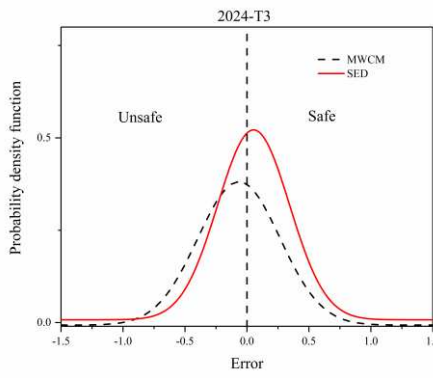
(a)



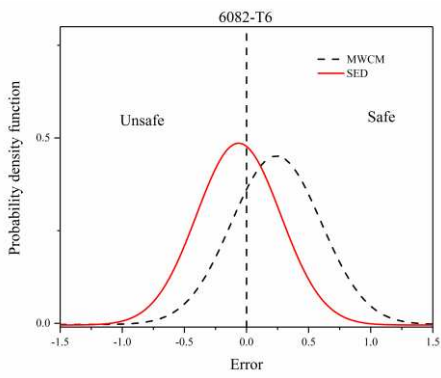
(b)



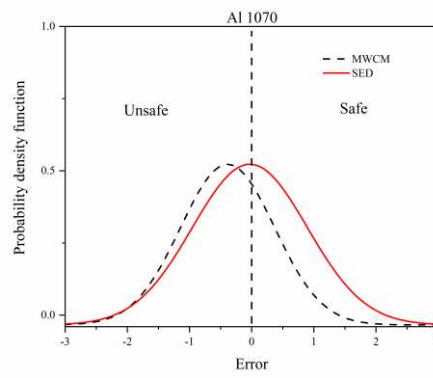
(c)



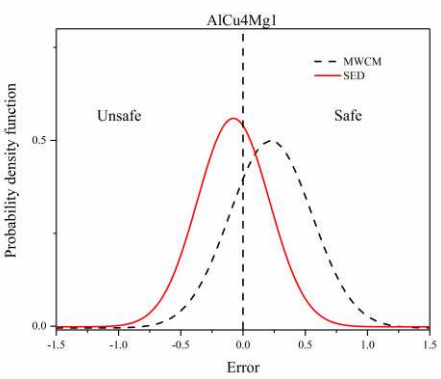
(d)



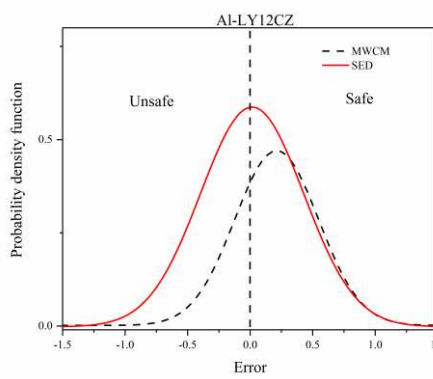
(e)



(f)



(g)



(h)

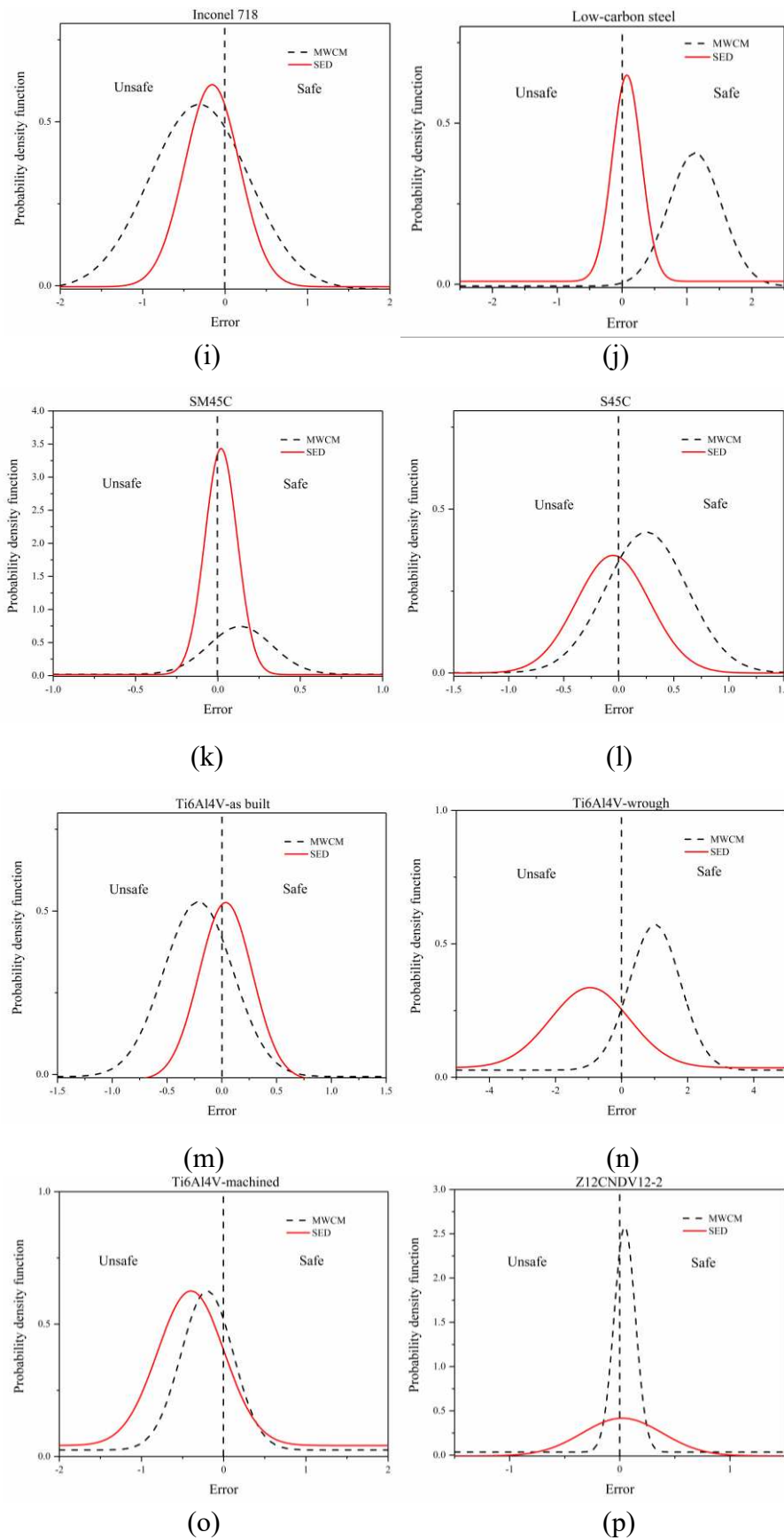
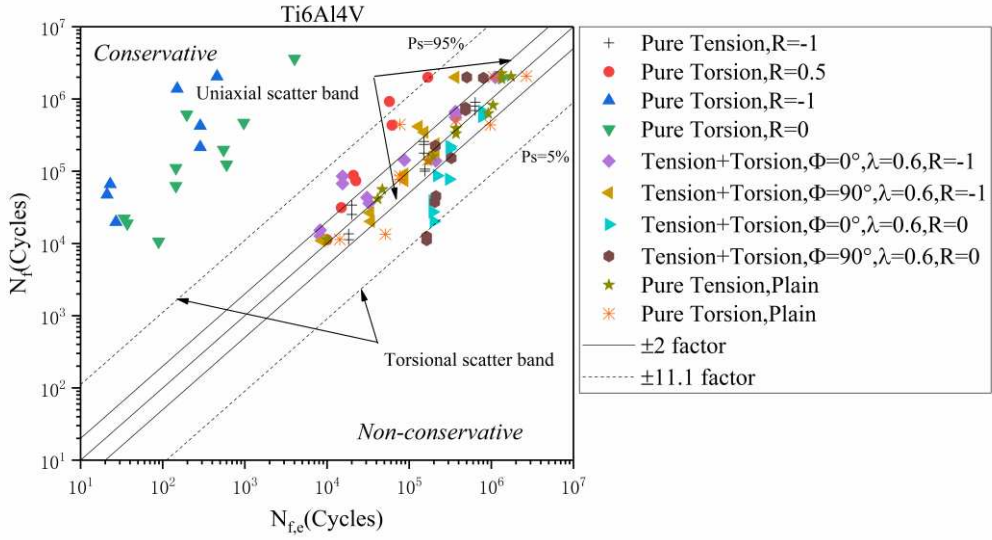
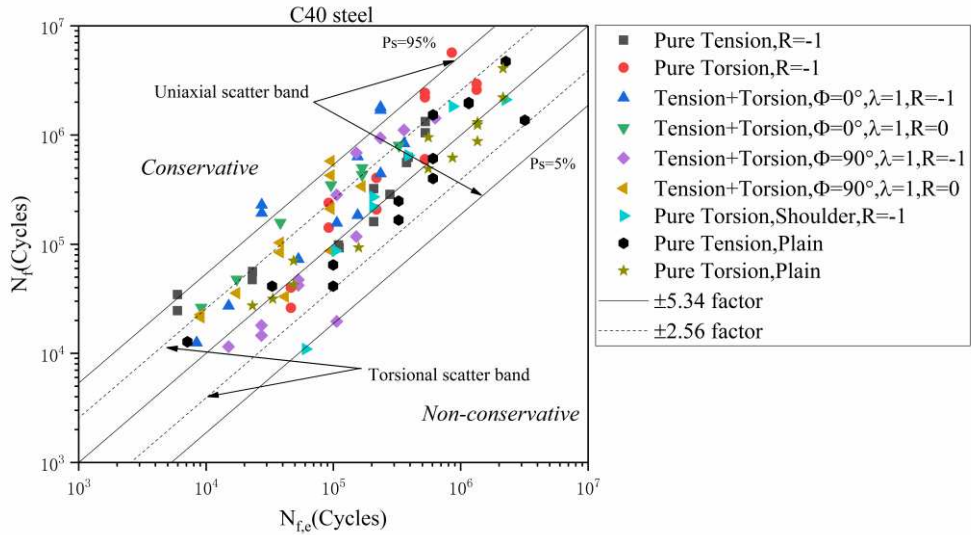


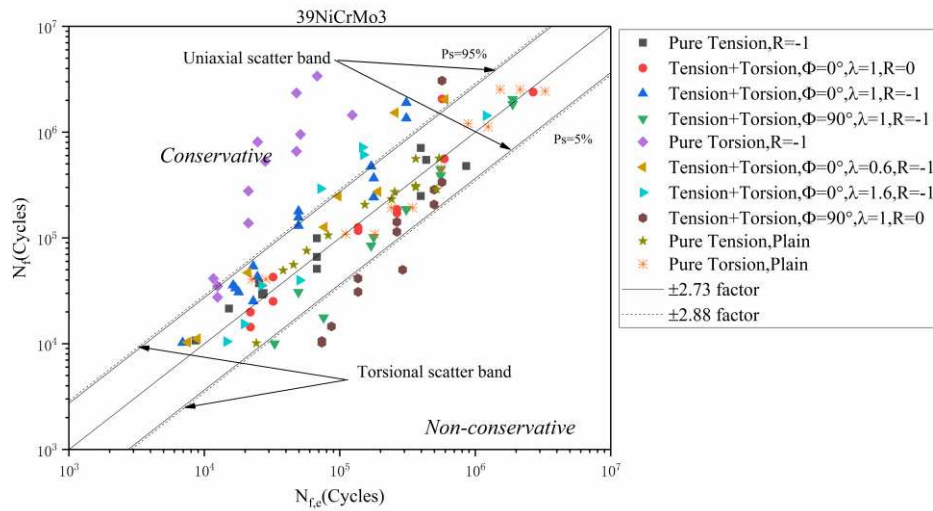
Figure 14 Probability density function of errors of predicting fatigue lifetime of plain specimens under multiaxial loading according to MWCM and SED.



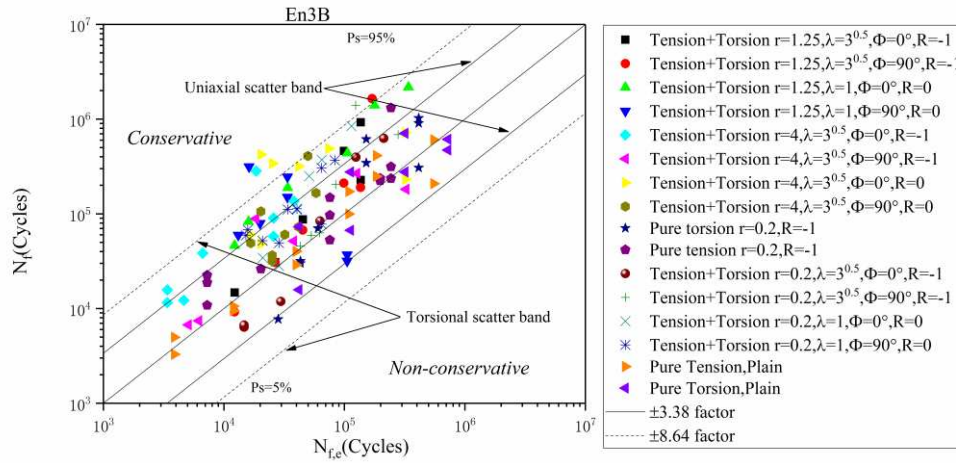
(a)



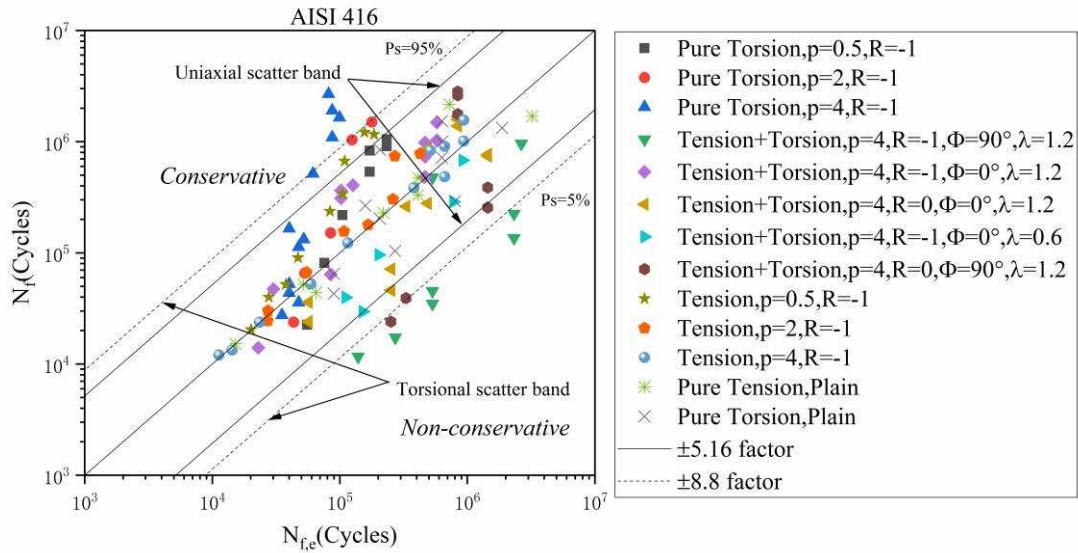
(b)



(c)

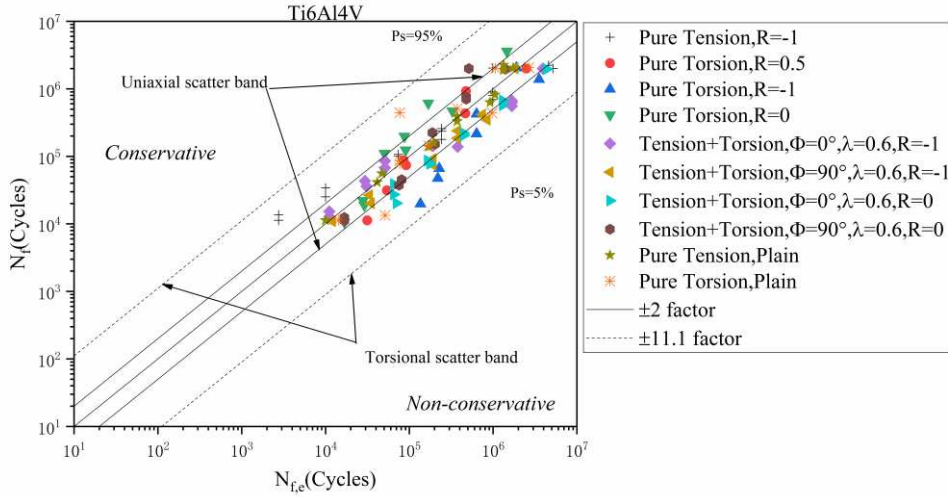


(d)

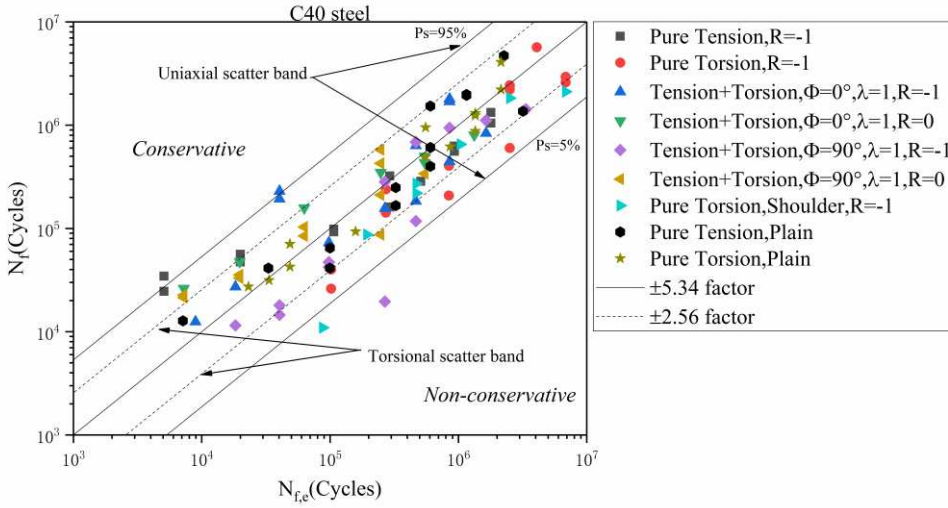


(e)

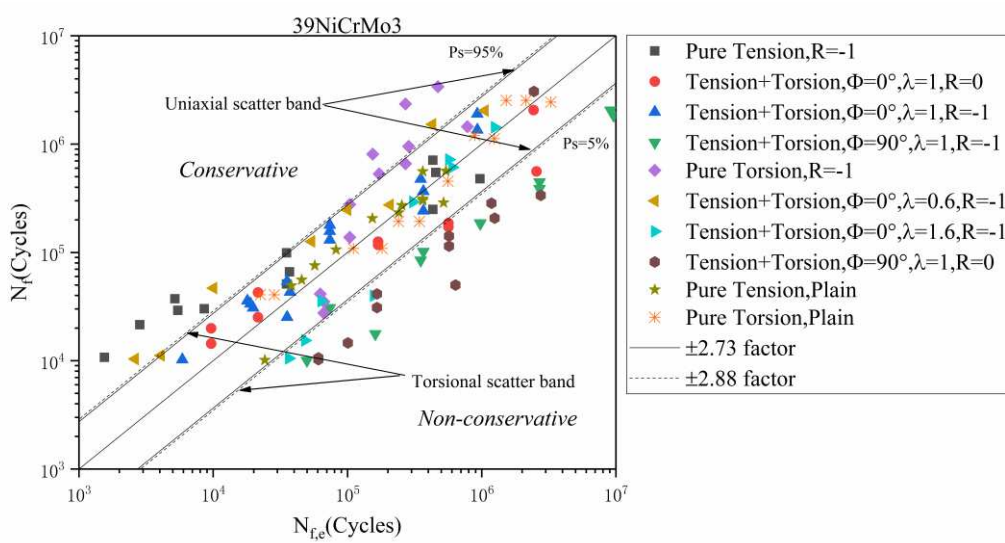
Figure 15 MWCM accuracy in predicting fatigue lifetime of notched specimens under multiaxial loading.



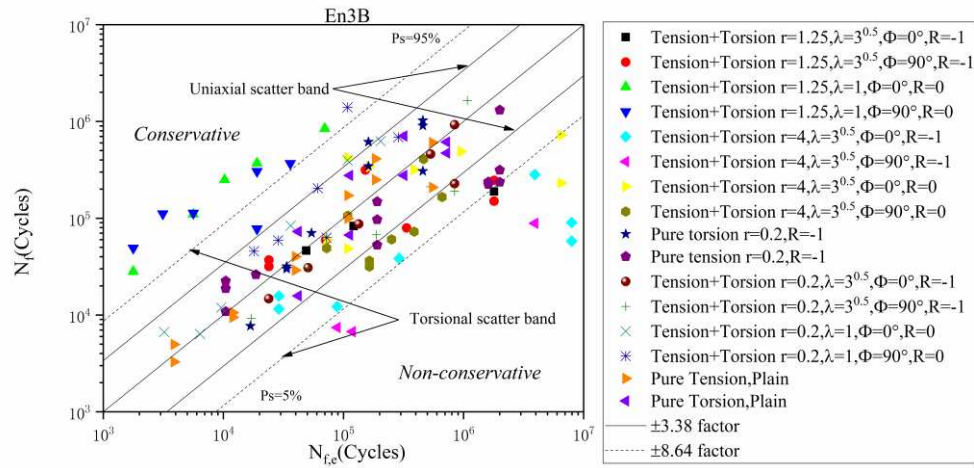
(a)



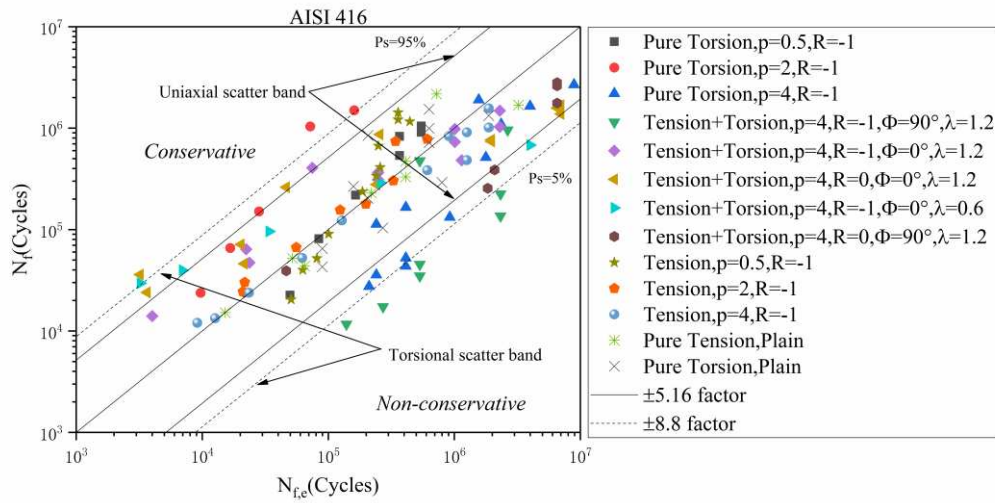
(b)



(c)

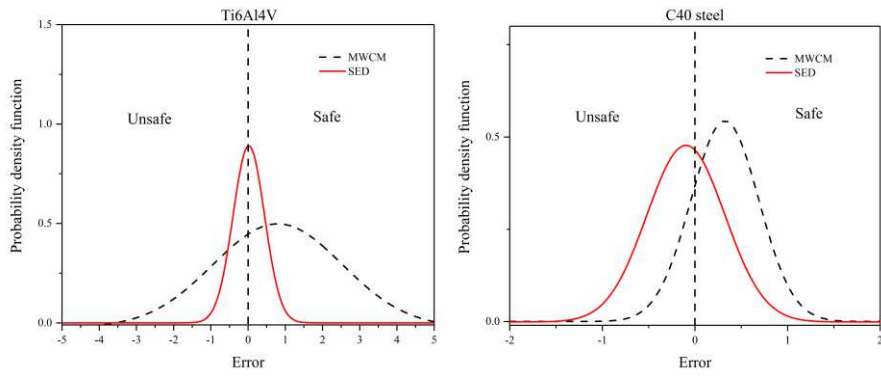


(d)



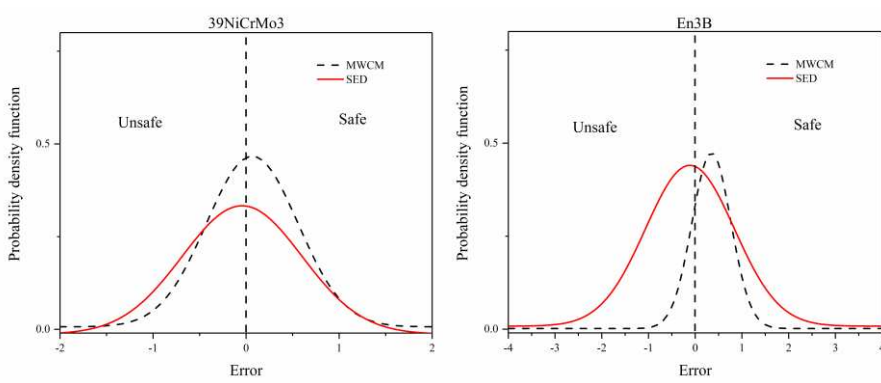
(e)

Figure 16 SED accuracy in predicting fatigue lifetime of notched specimens under multiaxial loading.



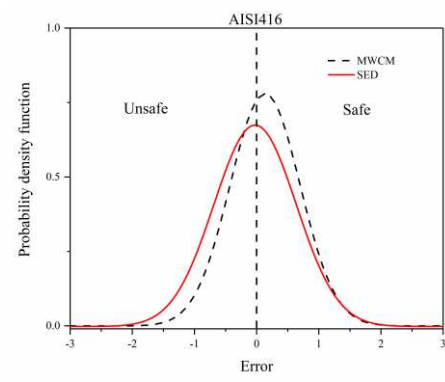
(a)

(b)



(c)

(d)



(e)

Figure 17 Probability density function of errors of predicting fatigue lifetime of notched specimens under multiaxial loading according to MWCM and SED.